Applied Thermal Engineering 299 (2026) 131179

Contents lists available at ScienceDirect

Applied Thermal Engineering

journal homepage: www.elsevier.com/locate/ate

Research Paper

Thermodynamic integration of HTGR nuclear heat into the Barrancabermeja Refinery

Nicolas Enciso [a,b,*], Daniel Morales [a,c]

[a] Grupo de Investigación en Ciencia y Tecnologías Nucleares, Red Nuclear Colombiana, Bogotá, Colombia
[b] Instituto de Pesquisas Energéticas e Nucleares (IPEN), São Paulo, Brazil
[c] TESLA Research Group, Universidad de Antioquia, Medellín, Colombia

ARTICLE INFO

Keywords:
High Temperature Gas-Cooled Reactor (HTGR)
Industrial heat applications
Process heat integration
Industrial decarbonization
Thermodynamic and exergy analysis
Nuclear heat

ABSTRACT

Decarbonizing refinery process heat and hydrogen production remains a major challenge for industrial net-zero pathways. High-temperature gas-cooled small modular reactors (HTGR–SMRs) are promising candidates because they combine high outlet temperatures, modular deployment, and inherent safety. This work develops a unified thermodynamic –exergy framework based on Pinch Point analysis, differential heat-transfer integration, and entropy-generation balances to assess HTGR coupling with refinery heat, hydrogen, and cogeneration systems under realistic industrial conditions. Results show that the main thermodynamic difference among the evaluated configurations is not the presence of the Once-Through Steam Generator (OTSG) itself, but the thermal matching between the nuclear heat source and refinery demands. Indirect steam delivery through an OTSG and direct helium supply to multiple refinery processes achieve comparable refinery-level performance, with second-law efficiencies of approximately 62.57%. In contrast, direct helium supply to the topping process – one of the most critical units in the refinery – reaches a lower efficiency of about 57.5%, corresponding to a relative improvement of approximately 8.8% for the OTSG and multi-process configurations. This indicates that, although direct helium exchange preserves a higher temperature potential, it suffers from greater thermal mismatch and higher irreversibility at the reactor–process interface, particularly when applied to single high-demand units such as topping. Applied to the Barrancabermeja Refinery, the proposed architecture could supply about 400 MW_{th} of process heat while supporting cogeneration, low-carbon hydrogen pathways, and avoiding on the order of 3 Mt CO_2/year.

1. Introduction

Achieving global net-zero emissions by mid-century requires deep transformations in how energy is produced and used across all sectors [1,2]. The industrial sector remains one of the most difficult to decarbonize because a large fraction of its energy demand is associated with continuous, high-temperature process heat still supplied predominantly by fossil fuels [3,4]. Within this challenge, refineries and petrochemical complexes are especially important because they combine large thermal loads, stringent temperature requirements, and substantial hydrogen demand in tightly integrated continuous-operation systems [5–7]. Refinery fired heaters and hydrogen plants based on Steam Methane Reforming (SMR-H_2) rank among the largest single-point CO_2 sources in industry, with typical emission intensities of 0.18–0.22 t CO_2/MWh_{th} and 8–10 kg CO_2/kg H_2, respectively [5,6].

These constraints motivate the search for low-carbon, high-grade heat sources suitable for continuous industrial operation. High-Temperature Gas-Cooled Reactors (HTGRs) in Small Modular Reactor (SMR) configurations have re-emerged as strong candidates, with helium-cooled outlet temperatures in the 700–750 °C range well aligned with refinery and hydrogen-process requirements, and modular architectures that allow incremental capacity addition, factory fabrication, and site-specific adaptation [8–10].

In parallel, light-water SMR vendors are beginning to target the same industrial segment: in 2026, NuScale Power and Ebara Elliott Energy announced a strategic partnership to develop and field test a commercial-scale high-temperature steam compressor for integrating NuScale Power Modules with petrochemical plants requiring process steam above 500 °C, explicitly framing SMR-derived steam as a decarbonization option for petrochemical process heat [11].

Among available HTGR designs, the HTR-PM and the Xe-100 stand out as the most relevant reference systems: the former provides an operationally demonstrated modular platform, while the latter is specifically positioned for industrial cogeneration and multi-unit deployment [12–15].

* Corresponding author at: Grupo de Investigación en Ciencia y Tecnologías Nucleares, Red Nuclear Colombiana, Bogotá, Colombia.
E-mail address: nicolas.enciso@rednuclearcolombiana.org (N. Enciso).

https://doi.org/10.1016/j.applthermaleng.2026.131179
Received 21 December 2025; Received in revised form 19 April 2026; Accepted 22 April 2026
Available online 25 April 2026

Abbreviations

HTGR	High-Temperature Gas-Cooled Reactor
SMR	Small Modular Reactor
HTGR–SMR	High-Temperature Gas-Cooled Small Modular Reactor
HTR-PM	High-Temperature Reactor–Pebble-bed Module
Xe-100	X-energy 100 MW_e Modular HTGR
OTSG	Once-Through Steam Generator
IHX	Intermediate Heat Exchanger
HPT	High Pressure Turbine
IPT	Intermediate Pressure Turbine
LPT	Low Pressure Turbine
GT	Gas Turbine
HRSG	Heat Recovery Steam Generator
LMTD	Log Mean Temperature Difference
CHT	Cumulative Heat–Temperature
CHP	Combined Heat and Power
HTSE	High-Temperature Steam Electrolysis
SMR-H_2	Steam Methane Reforming (hydrogen production process)
H_2	Hydrogen
FCC	Fluid Catalytic Cracking
CCR	Continuous Catalytic Reforming
HDT	Distillate Hydrotreating
VGO	Vacuum Gas Oil
TRISO	Tri-structural Isotropic (fuel particle)
LWR	Light Water Reactor
TRL	Technology Readiness Level
INL	Idaho National Laboratory
IAEA	International Atomic Energy Agency
MW_{th}	Thermal megawatt
MW_e	Electric megawatt
CO_2	Carbon Dioxide
CO_2-eq	Carbon Dioxide Equivalent

A recent closely related study by El-Emam et al. [16] develops a thermodynamic model for SMR integration into a generic petrochemical refinery via a steam Rankine cycle, demonstrating that nuclear-derived steam can supply a substantial fraction of refinery thermal demand and significantly reduce CO_2 emissions under full nuclear assistance [16]. The present study is complementary to and extends that work by explicitly comparing two heat-delivery architectures—direct helium coupling and indirect steam coupling through an OTSG—for two specific reactor designs (HTR-PM and Xe-100) and by applying them to a real refinery case (Barrancabermeja) with quantified heat, hydrogen, and cogeneration demands.

Despite this growing body of work, much less attention has been given to the detailed thermodynamic integration of specific HTGR–SMR designs with real refinery systems, where temperature matching, heat-transfer surface requirements, and exergy losses must be evaluated simultaneously under realistic process boundary conditions—particularly when comparing direct helium coupling against indirect steam-based configurations [8,17,18].

The analysis is grounded in the Barrancabermeja Refinery in Colombia, the country's largest refining facility, with a process heat demand of approximately 400 MW_{th} and direct emissions of 3.7 Mt CO_2-eq/year [6,19,20]. Two coupling pathways are evaluated: direct helium exchange, which defines the upper temperature potential of HTGR process heat but may incur large temperature mismatches, and indirect steam coupling through an OTSG, which improves thermal matching, preserves safety separation, and aligns with industrial practice [13,15,18]. The analysis extends to hydrogen production and cogeneration, capturing the full exergy-allocation problem of HTGR–SMRs in a complex industrial site.

Accordingly, the main contributions of this paper are threefold: (i) to develop a unified thermodynamic–exergy framework that provides a physically consistent second-law basis for HTGR–refinery integration, (ii) to apply this framework to compare alternative coupling architectures under realistic industrial boundary conditions, quantifying heat-transfer feasibility, required exchanger area, and irreversibility levels, and (iii) to clarify the role of reactor design and heat-delivery strategy in refinery decarbonization, using the Barrancabermeja Refinery as a representative large-scale case study [21–24].

The paper is organized as follows. Section 2 introduces the HTGR–SMR rationale and presents the HTR-PM and Xe-100 as reference systems. Section 3 develops the thermodynamic framework. Section 4 establishes the HTGR–OTSG thermodynamic baseline. Section 5 presents the refinery integration results. Section 6 extends the analysis to hydrogen production and cogeneration. Section 7 consolidates these results into an integrated deployment architecture for the Barrancabermeja Refinery. Finally, Section 8 summarizes the main findings.

2. Industrial context and reference HTGR systems

This section defines the industrial and technological boundary conditions of the present study. First, the Barrancabermeja Refinery is introduced as the reference industrial site, emphasizing its process-heat, hydrogen, and broader energy demands. Second, the two HTGR–SMR systems selected as reference nuclear heat sources – the HTR-PM and the Xe-100 – are presented in terms of their thermodynamic characteristics, design maturity, and suitability for refinery and hydrogen applications [6–8,25].

2.1. Barrancabermeja refinery: Heat, hydrogen, and energy demand

The Barrancabermeja Refinery, 100% owned and operated by Ecopetrol S.A., is the largest refining facility in Colombia and one of the most important industrial energy hubs in Latin America [19,20]. With a nominal capacity of approximately 250,000 barrels per day (12.4 Mt/year) and a Nelson complexity index of 6, it is classified as a medium-to-high complexity, cracking-type facility processing medium-to-heavy crude oils, supplying more than 40% of Colombia's liquid fuels [6,20,26]. Its process portfolio – atmospheric and vacuum distillation, FCC, visbreaking, catalytic reforming (CCR), hydrotreating, alkylation, and associated utility systems – forms a highly energy-intensive complex whose scale and process diversity make it a particularly relevant case for assessing HTGR–SMR integration [6,19,20].

From a thermodynamic perspective, Barrancabermeja is characterized by a large and heterogeneous demand for medium- and high-temperature process heat spanning roughly 200 to above 500 °C, encompassing crude preheating, vacuum distillation, FCC feed preheating, hydrotreating, catalytic reforming, and residual-product upgrading [6,19,27,28]. These temperature levels overlap significantly with the heat-delivery range of HTGR-based systems, particularly when indirect steam interfaces are employed to improve temperature matching and reduce exergy destruction [8,18,29]. Table 1 summarizes the principal process units, their operating conditions, and thermal demands considered in this study.

Atmospheric distillation represents the largest single thermal load, followed by FCC and vacuum distillation, while hydrotreating and upgrading units contribute medium-temperature demand [6,19,28,30]. Collectively, the core units define a heat-demand envelope of approximately 400 MW_{th}, consistent with the ~445 MW_{th} fired-heater duty reported for a generic 200,000 b/d refinery by the IEA GHG programme [31] and with current-average energy intensities of 81–264 kBtu/bbl per process unit compiled by the U.S. DOE [32].

In addition to process heat, Barrancabermeja has a substantial hydrogen demand from hydroprocessing, sulfur removal, and fuel-quality upgrading, met entirely through natural-gas steam methane reforming (SMR-H_2) [6,7]. According to the bottom-up refinery model of Yáñez et al. [6], the three existing hydrogen production units yield approximately 29,100 t H_2/year (≈80 t/day) with a combined emission factor

Table 1
Representative operating conditions and thermal power demand of major process units in the Barrancabermeja Refinery, illustrating the temperature levels and heat loads relevant for HTGR-based industrial heat integration [6,20,33,34].

Process Unit	ΔT (°C)	P (MPa)	Flow (kbpd/kg s^{-1})	Density (kg m^{-3})	Thermal power (MW$_{th}$)	Representative mixture
Atmospheric Distillation	30–370	0.10	232 / 363	850	415.48	Table 4
Vacuum Distillation	370–420	0.02	101 / 168	900	22.80	Table 5
Visbreaking	420–480	1.5	33 / 56	920	9.53	*n*-Tetradecane 0.15, *n*-Hexadecane 0.20, *n*-Octadecane 0.25, *n*-Eicosane 0.20, *n*-Heneicosane 0.10, *n*-Docosane 0.10
Fluid Catalytic Cracking (FCC)	480–520	0.25	84 / 131	850	16.68	*n*-Decane 0.25, *n*-Dodecane 0.25, Toluene 0.25, *n*-Octane 0.25
Catalytic Reforming (CCR)	400–480	3.5	10 / 13.8	750	3.42	*n*-Pentane 0.25, *n*-Hexane 0.25, *n*-Octane 0.20, Toluene 0.30
Distillate Hydrotreating (HDT)	300–350	8.0	57 / 85.7	820	11.14	*n*-Tetradecane 0.65, *n*-Hexadecane 0.35
VGO Hydrotreating	330–380	12.0	19.8 / 27.5	850	3.67	*n*-Tetradecane 0.30, *n*-Hexadecane 0.25, *n*-Octadecane 0.25, *n*-Eicosane 0.10, *n*-Heneicosane 0.05, *n*-Docosane 0.05
FCC Naphtha Hydrotreating	300–350	4.0	19 / 6.6	740	1.08	*n*-Pentane 0.30, *n*-Hexane 0.30, *n*-Octane 0.20, Toluene 0.20
Alkylation	50–80	2.5	2.1 / 0.41	700	0.03	*n*-Butane 0.50, *n*-Pentane 0.30, *n*-Hexane 0.20
Aromatics Extraction	130–150	0.6	2.2 / 0.76	750	0.04	Toluene 0.50, *n*-Octane 0.30, *n*-Decane 0.20
Base Oil Plant	250–300	1.0	0.9 / 0.52	920	0.07	*n*-Hexadecane 0.25, *n*-Octadecane 0.25, *n*-Eicosane 0.25, *n*-Heneicosane 0.15, *n*-Docosane 0.10
Asphalt Plant	150–200	0.5	6 / 4.17	970	0.48	*n*-Tetradecane 0.20, *n*-Octadecane 0.25, *n*-Eicosane 0.25, *n*-Heneicosane 0.15, *n*-Docosane 0.15

of ≈10.2 kg CO_2/kg H_2, contributing ≈297,000 t CO_2/year to the site's total GHG footprint of 3.7 Mt CO_2-eq/year [6]. These figures make the refinery a relevant benchmark for evaluating both nuclear process-heat substitution and nuclear-assisted hydrogen production through HTSE or hybrid preheating schemes [6,7,35].

Beyond heat and hydrogen, the refinery operates as a multi-vector energy hub. Steam and electricity are produced by a combined heat and power (CHP) system of three facility groups – two boiler–steam-turbine trains and a Gas Turbine (GT)–Heat Recovery Steam Generator (HRSG) unit – delivering approximately 2.42 PJ_e/year at a carbon intensity of ≈0.41 kg CO_2/kWh [6], more than three times the Colombian grid average. The steam network serves three pressure levels (600, 400, and 150 psi), with low-pressure steam accounting for 51% of process steam, medium-pressure for 33%, and high-pressure for 16% [6]. This multi-vector demand profile makes the refinery a suitable candidate for integrated nuclear energy supply, in which HTGR thermal output can be flexibly allocated among process heat, hydrogen production, and electricity generation [7,8,36].

From the standpoint of deployment strategy, Barrancabermeja offers a realistic scale for modular nuclear implementation: a single HTGR module would be insufficient to cover full refinery thermal demand, but multi-module deployment can match the site progressively [10,29,37]. This perspective is reinforced by Ecopetrol's active decarbonization program, which includes a US$ 1.2 billion investment for the LBCC clean-fuels project (2025–2030) and the inauguration of the 26 MW_p La Iguana solar farm at the refinery site [26,38], together with Colombia's national hydrogen roadmap [39]—all of which open a practical window for co-locating HTGR modules alongside new refinery infrastructure. Taken together, these characteristics make Barrancabermeja an especially strong case study for HTGR integration in an emerging-economy industrial context [6–8].

2.2. Reference HTGR systems: HTR-PM and Xe-100

HTGRs deployed at SMR scale provide a combination of high outlet temperature, favorable heat-transfer characteristics, intrinsic safety, and modular scalability that is particularly well suited to refinery and hydrogen applications [7,8,40]. Unlike conventional Light Water Reactors (LWRs), which are generally limited to outlet temperatures of about 300–320 °C, HTGRs employ helium coolant and graphite moderation to achieve core outlet temperatures typically around 700–750 °C [8,17,41]. This temperature range directly expands the class of industrial processes that can be supplied with nuclear heat, including crude distillation, hydrotreating, catalytic reforming, and advanced hydrogen production routes [8,29,30,35].

A central enabling feature of HTGR technology is the use of TRISO fuel, in which the fissile kernel is encapsulated within multiple ceramic coating layers that act as individual containment barriers [40,42]. Together with the chemical inertness and single-phase behavior of helium, this fuel concept provides large thermal safety margins and supports passive heat-removal behavior even under off-normal conditions [40,42]. When these reactors are deployed at SMR scale, the resulting systems also benefit from modular construction, shorter installation schedules, and the possibility of matching industrial demand through incremental multi-unit deployment rather than a single large reactor block [10,43].

These features are particularly important in refinery applications. First, the HTGR temperature range overlaps well with the main medium- and high-grade heat requirements of Barrancabermeja and similar complexes [6,8,19]. Second, modular deployment allows the reactor capacity to be distributed across large industrial sites in stages [10,43]. Third, the same reactor thermal output can support multiple energy products—process heat, electricity, and hydrogen—which is fully consistent with the integrated energy-demand profile described in Section 2.1 [7,25,36].

To represent the most realistic near-term HTGR deployment envelope, this study adopts two reference reactor systems: the Chinese HTR-PM and the American Xe-100. These designs were selected because they are among the most advanced and deployable HTGR–SMR concepts currently available and together span two complementary industrial deployment pathways: (i) a high-power, centrally deployed modular system and (ii) a smaller, more flexible factory-oriented modular system [8,12,14].

HTR-PM

The High-Temperature Reactor–Pebble-bed Module (HTR-PM) is a Chinese Generation IV HTGR developed by the Institute of Nuclear and

New Energy Technology (INET) at Tsinghua University in collaboration with China National Nuclear Corporation (CNNC) [12,13]. It builds on the operational experience of the 10 MW_{th} HTR-10 experimental reactor and constitutes the most mature deployable pebble-bed HTGR concept currently available [8,12,13].

The HTR-PM plant configuration comprises two reactor modules, each rated at 250 MW_{th}, coupled to a single steam turbine delivering approximately 210 MW_e net electrical power [13,29]. Helium serves as the primary coolant and graphite as the moderator, with core outlet temperatures of about 750 °C feeding an indirect steam cycle [8,13]. This configuration enables both electricity generation and industrial process-heat delivery, making the HTR-PM particularly relevant for large refinery complexes with high and relatively concentrated thermal demand [7,29].

A notable design feature of the HTR-PM is its online refueling capability using TRISO-fueled graphite pebbles circulating continuously through the core [13,40]. This contributes to stable long-term operation and is advantageous for industrial coupling, where thermal continuity is highly desirable [8,29]. From an application standpoint, the HTR-PM is especially well suited to centralized deployment in large sites such as Barrancabermeja, where multiple 250 MW_{th} modules can be clustered to cover substantial fractions of refinery heat demand while preserving high-grade exergy for hydrogen production or power generation [7,29].

Xe-100

The Xe-100 is a modular HTGR developed by X-energy in the United States and represents a more compact but highly scalable interpretation of the HTGR–SMR concept [14,37]. Like the HTR-PM, it uses helium cooling, graphite moderation, and TRISO fuel, but it is designed around 200 MW_{th} reactor modules producing approximately 80 MW_e each [14,15].

The Xe-100 also operates with outlet temperatures in the HTGR range and includes an indirect steam interface suitable for industrial heat delivery and hydrogen-related applications [14,18]. Its secondary system can support OTSG operation at conditions appropriate for process-steam supply or hydrogen production via HTSE [14,18]. Because of its lower unit power and intended modular factory-based deployment model, the Xe-100 is particularly attractive for phased installation, industrial parks, and distributed energy applications where capacity may need to expand progressively [10,37].

From the perspective of refinery integration, the Xe-100 defines a complementary pathway to the HTR-PM. Whereas the HTR-PM favors large centralized sites with major concentrated loads, the Xe-100 offers greater flexibility for staged deployment and can be aggregated in multi-unit configurations to match demand growth or retrofit limitations [14,37]. This makes it a useful comparative benchmark for evaluating how reactor size and modular strategy affect heat-transfer matching and exergy performance at the refinery interface [8,18].

Comparison of key thermodynamic and design parameters

The principal thermodynamic and structural parameters of both systems are summarized in Table 2. These parameters define the upper temperature limits, available heat duty per module, and overall deployment characteristics used throughout the subsequent analysis [10,13,15,44].

The comparison indicates that both reactor systems are thermodynamically compatible with the temperature range of the refinery services considered in this study [8,18,29]. Their common 750 °C outlet temperature enables coupling with a broad spectrum of refinery and hydrogen applications, while differences in thermal power, mass flow rate, and deployment scale mainly affect exchanger sizing, modularization strategy, and phasing rather than the fundamental feasibility of integration [13,14].

From an engineering standpoint, the HTR-PM and Xe-100 should therefore be interpreted not as competing in a purely binary sense, but as defining the realistic design envelope of near-term HTGR–SMR deployment for industrial decarbonization [7,8]. The HTR-PM represents the reference case for large-scale, centralized refinery integration, whereas the Xe-100 represents a modular pathway more readily aligned with phased build-out and distributed industrial energy systems [29,37].

3. Thermodynamic analysis framework

This section presents the integrated methodological framework used to evaluate the thermodynamic feasibility and second-law performance of coupling HTGR–SMRs with refinery process-heat, hydrogen, and cogeneration systems. Building on the industrial context of the Barrancabermeja Refinery and the reference reactor conditions introduced in Section 2, the framework combines Pinch Point analysis, differential heat-transfer evaluation, and entropy–exergy balances within a unified approach [8,18,21].

The objective of the framework is not only to determine whether a given reactor–process coupling is thermodynamically feasible, but also to quantify how temperature matching, required heat-transfer area, and irreversibility levels vary across alternative integration pathways. This is particularly important in refinery systems, where broad heat demand distributions, multicomponent hydrocarbon streams, and phase transitions make simplified constant-temperature or constant-c_p approximations inadequate [25,28,30].

All calculations are referenced parametrically to the two HTGR–SMR systems selected as industrial benchmarks in this work: the HTR-PM and the Xe-100. These systems define the reactor-side thermal boundary conditions for the subsequent analyses and enable the same methodology to be applied consistently across high-power and medium-power modular deployment scenarios [13–15].

The analysis proceeds through three sequential and interdependent steps:

- Definition of a reference reactor–process interface based on an indirect OTSG, which establishes the common thermal boundary conditions used throughout the study.
- Heat-exchange characterization through Pinch Point analysis and differential heat-transfer integration, used to quantify temperature matching, feasible heat transfer, and exchanger area requirements.
- Quantification of irreversibilities through entropy-generation and exergy-destruction balances, enabling direct comparison of coupling strategies on a second-law basis.

Pinch Point analysis identifies the minimum temperature approach and thermodynamic limit of feasible heat transfer, differential heat-transfer integration links local thermal driving forces to exchanger sizing, and exergy analysis quantifies the degradation of available work associated with temperature mismatch and heat-transfer irreversibility [22–24,45,46]. Together, these methods provide a thermodynamically consistent basis for comparing direct helium coupling, indirect steam coupling, and hybrid industrial integration pathways under realistic engineering constraints.

Thermophysical properties were evaluated in a `Python` environment using the `CoolProp` adn `CANTERA` librarys and, with steady-state operation, countercurrent heat exchange, and negligible pressure-drop and radiative losses assumed throughout the baseline assessment. These assumptions define a first-order feasibility envelope suitable for comparative design analysis rather than detailed final engineering design [24,47,48].

3.1. Reference system configuration: HTGR with once-through steam generator

The thermodynamic reference system adopted in this work is an indirect heat-delivery configuration in which the reactor primary helium

Table 2
Main design and thermodynamic parameters of the HTR-PM and Xe-100 HTGR–SMR concepts, used in this work as reference boundary conditions for refinery and hydrogen integration analyses [10,13,15,44].

Parameter	HTR-PM (per module)	Xe-100 (per module)	Unit
Thermal Power	250	200	MW_{th}
Electrical Power (net)	105	80	MW_e
Core Outlet Temperature	750	750	°C
Core Inlet Temperature	250	260	°C
Primary Coolant	Helium	Helium	–
Primary Coolant Pressure	7.0	6.0	MPa
Coolant mass flow rate	96.35	78.6	kg/s
Secondary fluid mass flow rate	89.81	76.6	kg/s
Fuel Type	TRISO (UO_2)	TRISO (UCO)	–
Moderator/Structure	Graphite	Graphite	–
Steam Cycle Interface	OTSG–Rankine	OTSG–Rankine	–
Design Maturity (TRL)	9	7–8	–

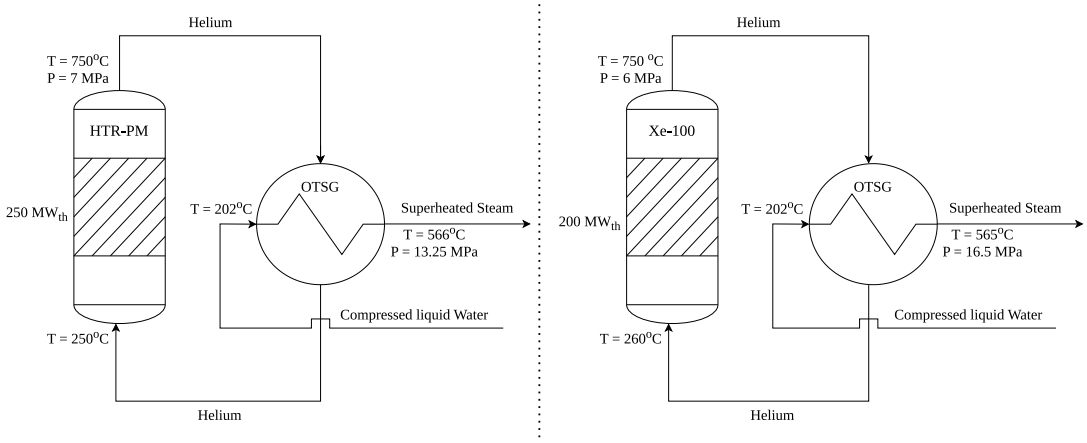

Fig. 1. Simplified process-flow diagram of the HTR-PM and Xe-100 systems in Once-Through Steam Generator (OTSG) configuration, showing the primary helium loop, secondary steam circuit, and the thermal interfaces that define the boundary conditions for industrial heat integration and cogeneration analyses.

loop transfers heat to a secondary steam circuit through an OTSG. This secondary loop then acts as the interface between the nuclear system and the downstream industrial process network [13,15,18].

This configuration was selected over direct helium–process coupling for three principal reasons. First, it improves safety by preserving hydraulic and radiological separation between the nuclear and industrial domains. Second, it mitigates materials and corrosion constraints associated with direct high-temperature helium exchange. Third, it aligns with the reference layouts already adopted in both the HTR-PM and Xe-100 concepts, making it a credible near-term integration pathway for refinery and hydrogen applications [8,14,18].

The OTSG architecture preserves a large fraction of the high-temperature potential of the HTGR while using a mature steam interface that is compatible with refinery heaters, hydrogen production systems, and cogeneration schemes. In practical terms, it also provides a convenient common boundary condition for comparing reactor concepts of different size without altering the downstream thermodynamic methodology [7,36].

Table 2 summarize the reference operational parameters used for the HTR-PM and Xe-100 systems, respectively. Both designs are modeled with helium outlet temperatures of 750 °C, defining the upper thermal boundary condition for all industrial integration cases considered in this work [13,15].

Fig. 1 illustrates the simplified reference configuration used throughout the methodological development. The scheme highlights the primary helium loop, the OTSG heat-transfer stage, and the secondary steam interface through which heat is ultimately delivered to refinery and hydrogen systems.

This reference configuration defines the common thermal starting point for all subsequent analyses. Its thermodynamic performance is first evaluated as a component-level baseline in Section 4, after which the same boundary conditions are extended to the refinery, hydrogen, and cogeneration cases.

3.2. Pinch point methodology

Pinch Point analysis was used to identify the thermodynamic feasibility limits of heat exchange between reactor-side and process-side streams. In the present context, the key indicator is the minimum temperature difference, $\Delta T_{\min}$, which marks the point of closest thermal approach between the hot and cold streams and therefore defines the limiting constraint for feasible heat transfer [45,46].

While classical pinch analysis is typically applied to full heat-exchanger networks, in this work the methodology is adapted to single heat exchangers and localized reactor–process interfaces. This modification is important because the objective is not to synthesize a complete refinery network, but rather to evaluate the detailed thermodynamic compatibility of specific HTGR coupling schemes under realistic temperature trajectories and, where relevant, phase change [18,21,28].

The analysis is based on cumulative heat–temperature (CHT) curves, which represent the temperature evolution of the hot and cold streams as a function of cumulative transferred heat. For a stream with mass flow rate $\dot{m}$ and specific heat capacity c_p, the cumulative heat flow is written as

$$Q(T) = \int_{T_{\text{in}}}^{T} \dot{m}\, c_p\, dT. \tag{1}$$

The local temperature difference between the hot and cold streams is then expressed as

$$\Delta T(Q) = T_h(Q) - T_c(Q), \tag{2}$$

and the pinch condition is defined by

$$\Delta T_{\min} = \min_{Q} \Delta T(Q). \tag{3}$$

This representation makes it possible to identify not only the minimum approach temperature, but also the global thermal matching quality over the entire exchanger duty. For HTGR integration studies, this is particularly useful because helium and refinery process streams often exhibit very different effective heat-capacity rates, producing strongly nonuniform temperature differences even when inlet and outlet conditions appear acceptable [25,27,30].

Beyond identifying $\Delta T_{\min}$, the CHT representation provides direct information about where local thermal mismatch becomes most severe along the duty path. For that reason, pinch analysis serves as the natural bridge between feasibility assessment, exchanger sizing, and second-law interpretation in the integrated framework developed here [21–23].

3.3. Heat-transfer evaluation via differential heat-transfer integration

To translate the temperature profiles obtained from pinch analysis into engineering requirements, the present work uses a differential heat-transfer formulation rather than a single global Log Mean Temperature Difference (LMTD). This choice reflects the strong variation of local thermal driving force along the exchanger, especially in systems involving helium on one side and water/steam or multicomponent hydrocarbon streams on the other [24,49].

The local heat-transfer relation is written as

$$dQ = U\,\Delta T\,dA, \tag{4}$$

where U is the overall heat-transfer coefficient, ΔT is the local temperature difference, and dA is the incremental heat-transfer area. Rearranging, the local area contribution becomes

$$dA = \frac{dQ}{U(T_h - T_c)}. \tag{5}$$

Integration over the total exchanger duty yields the required heat-transfer area:

$$A = \int_0^{Q_{\max}} \frac{dQ}{U(Q)\,[T_h(Q) - T_c(Q)]}. \tag{6}$$

This formulation preserves the local thermal structure of the exchanger and is therefore better suited than a single LMTD value for systems with nonuniform temperature gradients or phase transitions. It also provides a direct physical connection between the pinch curves and exchanger sizing, since the same local temperature field used to determine $\Delta T_{\min}$ is integrated to calculate area [24,49,50].

For the helium–water OTSG reference case, the overall heat-transfer coefficient is treated as a piecewise function of the thermodynamic region of the water/steam side. The secondary fluid is divided into three practical regions:

- Subcooled liquid: $T < T_{\text{sat}}$
- Boiling region: $T \approx T_{\text{sat}}$
- Superheated vapor: $T > T_{\text{sat}}$

Accordingly, the local overall coefficient is written as

$$U(Q) = \begin{cases} U_L, & Q \in \Omega_L \\ U_{TP}, & Q \in \Omega_B \\ U_V, & Q \in \Omega_S \end{cases} \tag{7}$$

where Ω_L, Ω_B, and Ω_S denote the subcooled, boiling, and superheated regions, respectively.

Representative values were selected from standard ranges reported for gas–water heat exchange:

$$U_L = 800 \text{ W m}^{-2}\text{K}^{-1}, \tag{8}$$

$$U_{TP} = 1500 \text{ W m}^{-2}\text{K}^{-1}, \tag{9}$$

$$U_V = 600 \text{ W m}^{-2}\text{K}^{-1}. \tag{10}$$

These values reflect the expected enhancement of heat transfer in the boiling region and the lower convective coefficients in single-phase liquid and superheated vapor regions [24,50]. Numerically, the integral in Eq. (6) is evaluated using the trapezoidal rule along the cumulative heat coordinate, ensuring consistency with the same thermodynamic discretization adopted for the pinch analysis.

The advantage of this formulation is that it can be extended naturally to process-side cases involving crude oil and refinery mixtures, where neither c_p nor effective heat-transfer coefficients remain constant along the heating path. In that sense, the method provides a flexible but still physically transparent basis for comparing different HTGR coupling strategies at a common level of engineering detail [28,30,48].

3.4. Entropy generation analysis in the heat exchanger

The entropy generation associated with the heat exchange process was evaluated in order to quantify the thermodynamic irreversibilities of the system. For a steady-state control volume, the entropy balance can be expressed as

$$\dot{S}_{gen} = \sum_{out} \dot{m}s - \sum_{in} \dot{m}s - \sum \frac{\dot{Q}}{T} \tag{11}$$

where $\dot{S}_{gen}$ is the rate of entropy generation, $\dot{m}$ represents the mass flow rate, s is the specific entropy, and $\dot{Q}$ denotes the heat transfer occurring at the boundary temperature T.

For the heat exchanger considered in this work, heat transfer with the external environment is neglected, and therefore the system can be treated as adiabatic. Under this assumption, the entropy balance simplifies [7,22,23].

The associated exergy-destruction rate follows directly from the Gouy–Stodola theorem:

$$\dot{X}_{\text{dest}} = T_0 \dot{S}_{\text{gen}}, \tag{12}$$

where T_0 is the ambient reference temperature.

In the present work, these quantities are used as the principal indicators of thermodynamic irreversibility at the reactor–process interface.

Entropy generation captures the cumulative effect of local temperature differences over the exchanger duty. Exergy destruction, in turn, expresses the same effect in power units, making it especially useful for comparing the thermodynamic penalty of process heat delivery against alternative uses of reactor thermal output such as electricity generation or hydrogen production [7,22,23].

The combined use of Pinch Point analysis, differential heat-transfer integration, and exergy balances makes it possible to interpret each integration case at three distinct but connected levels:

- the **feasibility level**, through $\Delta T_{\min}$,
- the **equipment level**, through required exchanger area A,
- the **second-law level**, through $\dot{S}_{\text{gen}}$ and $\dot{X}_{\text{dest}}$.

This three-level interpretation is one of the central methodological contributions of the present work. Rather than evaluating heat-transfer feasibility, exchanger size, and exergy losses separately, the framework connects them through a common set of local temperature profiles and thermophysical-property calculations. This enables direct comparison between alternative HTGR integration schemes under a unified thermodynamic basis [8,18,21].

This framework is first applied in Section 4 to the helium–water OTSG baseline in order to establish the component-level thermodynamic reference of the intermediate steam loop. This same methodology is then extended in Section 5 to refinery process heating and in Section 6 to hydrogen production and cogeneration, allowing all cases to be interpreted on a common thermodynamic basis.

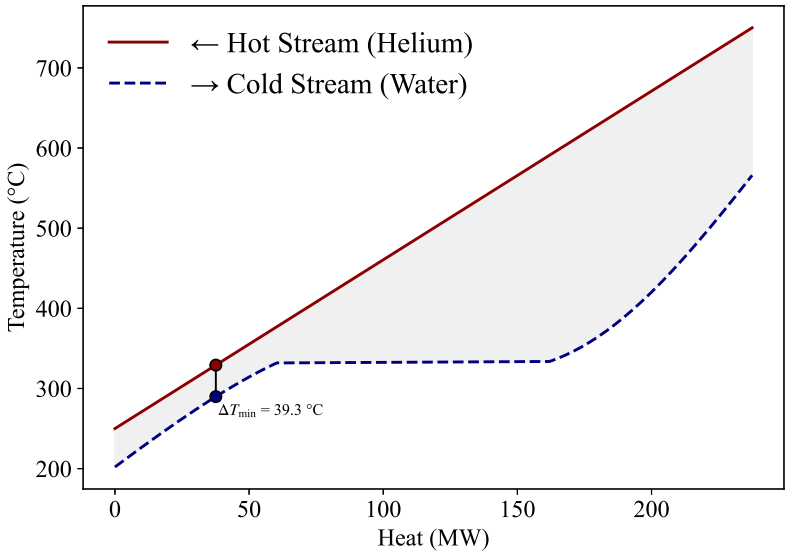

Fig. 2. Cumulative heat–temperature (CHT) curves for helium–water countercurrent heat exchange in the reference HTGR–OTSG system ($\varepsilon = 0.95$), identifying the pinch region and the minimum temperature difference that constrain feasible heat transfer and govern entropy generation.

4. Reference HTGR–OTSG baseline results

This section applies the thermodynamic framework developed in Section 3 to the reference HTGR–OTSG interface defined as the common delivery architecture for all subsequent industrial integration cases. The purpose of this baseline analysis is to establish the thermodynamic behavior of the helium–water/steam exchanger before refinery process streams are introduced. In this way, the component-level performance of the nuclear-to-steam interface can be separated from the additional irreversibilities associated with crude oil heating, multicomponent hydrocarbon mixtures, and hydrogen production pathways.

The reference case represents the indirect heat-transfer configuration already adopted as the preferred common boundary condition for the HTR-PM and Xe-100 systems. Helium exits the reactor at 750 °C and transfers heat to the secondary water/steam stream in a countercurrent on OTSG with an exchanger effectiveness of $\varepsilon = 0.95$. The resulting temperature profiles, required heat-transfer area, and entropy-generation levels define the baseline against which all refinery and hydrogen integration options are compared.

This section is organized in three parts. First, the thermal matching behavior of the helium–water OTSG is discussed using CHT curves. Second, the implications of the local temperature field for heat-transfer area are interpreted in engineering terms. Third, the associated entropy generation and exergy destruction are used to determine whether the intermediate steam loop is itself a major thermodynamic penalty or, instead, an effective exergy-conditioning stage between the reactor and the industrial process network.

4.1. Temperature matching in the reference OTSG

The first step in evaluating the reference HTGR–OTSG system is to determine the thermal compatibility between the reactor helium stream and the secondary water/steam circuit. Fig. 2 presents the CHT obtained for the helium–water countercurrent exchanger under the baseline conditions defined in Section 3.1. The hot and cold composite curves approach one another smoothly, and the pinch region remains localized rather than extending across a broad fraction of the exchanger duty.

The resulting minimum temperature difference is 39.3 °C, which is small compared with the values later obtained for direct helium coupling to refinery hydrocarbons. This indicates good thermal compatibility between the reactor-side helium and the steam generation duty. Physically, the reason is that water/steam offers a more favorable heat absorption trajectory than crude oil: boiling and superheating allow the cold-side stream to absorb heat over a temperature profile that better matches the helium enthalpy decline.

From the standpoint of heat integration, this result is significant because it shows that the indirect steam loop does not inherently create a severe pinch limitation. On the contrary, it converts the very high-grade thermal output of the reactor into a secondary thermal carrier with a much more adaptable temperature profile. This supports the use of the OTSG not merely as a safety-driven separation stage, but as a thermodynamically useful conditioning interface for downstream industrial applications.

4.2. Heat-transfer area and engineering implications

The local temperature field represented by the CHT curves can be translated into equipment requirements through the differential heat-transfer integration described in Section 3.3. For the reference helium–water case, the total heat-transfer area required to satisfy the specified duty at $\varepsilon = 0.95$ is 3119.6 m^2, obtained from Eq. (6) using the CHT profiles shown in Fig. 2. This result, summarized in Table 3, is consistent with an industrial-scale Intermediate Heat Exchanger (IHX) and indicates that the temperature approach achieved in the OTSG does not require unrealistically large heat-transfer surfaces.

The area requirement must be interpreted together with the distribution of local heat-transfer coefficients. In the OTSG, the boiling region contributes strongly to heat transfer because of its elevated effective coefficient, while the subcooled and superheated regions impose the main surface penalties. Even so, the overall area remains moderate when compared with the much larger exchanger demands associated with refinery process-side mismatches. This is important because it shows that the indirect steam interface improves thermal quality without making the exchanger physically prohibitive.

From a design perspective, the reference OTSG therefore occupies a favorable middle ground. It preserves much of the reactor temperature potential, provides a familiar steam interface for industrial systems, and does so with exchanger dimensions compatible with large nuclear and petrochemical equipment practice. This makes the helium–water baseline a credible engineering reference for both HTR-PM and Xe-100 deployment scenarios.

Table 3
Integrated thermodynamic performance indicators for the reference helium–water heat exchanger, combining Pinch Point, differential heat-transfer integration, and exergy analyses to quantify thermal matching, heat-transfer requirements, and irreversibility levels.

Parameter	Units	Value
Pinch-point temperature difference (ΔT_{min})	°C	39.3
Heat-transfer area (A)	m^2	3119.6
Entropy-generation rate ($\dot{S}_{gen}$)	kW/K	52.28
Exergy-destruction rate aprox. ($\dot{X}_{dest}$)	MW	15.59

4.3. Entropy generation and baseline exergy performance

The second-law performance of the reference exchanger is characterized by the entropy generation and exergy destruction along the helium–water heat-transfer path. For the baseline OTSG case, the entropy-generation rate is 52.28 kW/K, according to Eq. (11), and the exergy-destruction rate is 15.59 MW, as calculated from Eq. (12). These results suggest that the intermediate steam loop imposes a modest thermodynamic penalty and does not govern the irreversibility of the integrated system, particularly relative to the larger losses identified later in the direct reactor-to-refinery coupling configuration.

Table 3 compiles the principal indicators of the baseline OTSG performance. Considered together, the values show a coherent thermodynamic picture: a relatively low pinch-point temperature difference, a feasible exchanger area, and a moderate exergy penalty. In other words, the OTSG acts as an efficient exergy-conditioning stage, transforming reactor heat into a more usable industrial form while sacrificing only a limited fraction of available work.

These baseline indicators are essential for interpreting the refinery integration results. If the IHX had already imposed a large irreversibility penalty, the advantages of indirect steam coupling at refinery scale would be questionable. However, the present results show the opposite: most of the additional exergy destruction observed in direct industrial coupling arises not in the nuclear steam-generation stage, but in the mismatch between the heat-delivery medium and the refinery process stream itself.

The reference OTSG baseline therefore provides the thermodynamic foundation for the comparative analyses developed in the next sections. It establishes that the intermediate steam loop is both physically realistic and thermodynamically efficient, justifying its use as the preferred near-term delivery architecture for refinery heat, hydrogen support, and cogeneration integration.

4.4. Implications for subsequent integration cases

The baseline results of this section define the benchmark from which the more demanding industrial cases must be assessed. In practical terms, they show that a helium outlet temperature of 750 °C can be transferred to a secondary steam circuit with good temperature matching and moderate exergy loss, thereby preserving a large share of the reactor's useful thermal potential for downstream applications. This benchmark is especially important when evaluating direct helium coupling, because it isolates the penalty associated with bypassing the intermediate steam loop.

Taken as a whole, the present section shows that the indirect HTGR–OTSG interface should be interpreted not as an auxiliary component but as the central thermodynamic backbone of the integrated system. By establishing a low-irreversibility bridge between the reactor and the industrial site, it enables the comparative assessment of refinery heat, hydrogen, and cogeneration options on a common and physically meaningful basis.

Building on this baseline, Section 5 applies the same reactor-side thermal conditions to refinery process-heat duties, and Section 6 extends the framework to hydrogen production and cogeneration, where the value of preserving high-grade exergy becomes even more pronounced.

5. HTGR–refinery integration scenarios

This section develops the refinery integration scenarios built upon the component-level baseline established in Section 4. The objective is to evaluate how the reference HTGR thermal interface performs when extended from the helium–water/steam exchanger to representative refinery duties, with particular emphasis on atmospheric distillation, vacuum heating, and refinery-scale heat substitution in the Barrancabermeja case [6,19,28,30].

All scenarios are referenced to the reactor conditions defined in Section 2.2 and the thermal interface introduced in Section 3.1. Accordingly, the direct helium and indirect steam cases are assessed under a consistent reactor outlet condition of 750 °C, corresponding to the reference HTR-PM and Xe-100 boundary conditions. This consistency is essential for comparing integration pathways on a like-for-like thermodynamic basis [13–15].

The refinery-side analysis is organized in four steps. First, representative hydrocarbon mixtures are defined for the main process streams used in the topping and vacuum-heater cases. Second, direct helium coupling is examined as the upper-bound reactor–process integration route. Third, a multi-stage direct-heating configuration is evaluated to determine whether process-side heat cascading can mitigate the limitations of single-stage coupling. Fourth, an indirect steam-based OTSG configuration is assessed as the practical integration option under refinery-relevant conditions.

5.1. Representative hydrocarbon mixtures and thermophysical modeling

A central difficulty in refinery heat-integration studies is that actual process streams are multicomponent hydrocarbon mixtures with broad boiling distributions, non-ideal behavior, and composition ranges that are seldom reported in sufficient detail for reproducible thermodynamic modeling [25,28,48]. For this reason, the present work adopts representative surrogate mixtures for the refinery-side streams considered in the topping and vacuum heating cases. These mixtures are intended to preserve the relevant thermal behavior of the corresponding refinery cuts while remaining compatible with the property models available in `CoolProp` [21,47].

The topping-duty stream is represented by a light-to-medium hydrocarbon mixture dominated by *n*-alkanes in the C_5–C_{12} range, together with a limited aromatic fraction. This approximation reflects the composition of crude fractions entering or crossing the atmospheric-distillation heating interval, where the relevant thermal behavior is governed primarily by sensible heating below the heavy-residue regime [19,28,30]. The representative composition used in this work is summarized in Table 4.

The vacuum-heater stream requires a heavier surrogate because the relevant process duty is associated with the heating of vacuum gas oil and heavier residual fractions. In this temperature region, the effective heat capacity and density trends differ from those of lighter topping cuts, so a heavier pseudo-mixture must be used to preserve the correct thermodynamic response [6,19,30]. The representative heavy mixture adopted here is summarized in Table 5.

For the heavier fraction range (C_{13}–C_{22}), the thermophysical behavior was additionally simulated using `Cantera` to ensure a more consistent representation of high-temperature properties.

Table 4
Representative light-to-medium hydrocarbon surrogate mixture used for the atmospheric-distillation and topping-heater analyses, selected to approximate the thermal behavior of refinery streams in the medium-temperature heating range.

Component	Formula	Fraction type	Mass fraction (%)
n-Pentane	C_5H_{12}	Light gasoline cut	15
n-Hexane	C_6H_{14}	Intermediate gasoline	25
Toluene	C_7H_8	Aromatic fraction	15
n-Octane	C_8H_{18}	Heavy gasoline	20
n-Decane	$C_{10}H_{22}$	Kerosene/diesel cut	25

Table 5
Representative heavy hydrocarbon surrogate mixture used for vacuum-distillation and residue-heating analyses, selected to approximate the thermal response of heavier refinery fractions under medium- and high-temperature heating conditions.

Component	Formula	Fraction type	Mass fraction (%)
Tetradecane	$C_{14}H_{30}$	Heavy diesel fraction	20
Hexadecane	$C_{16}H_{34}$	Atmospheric gas oil	20
Octadecane	$C_{18}H_{38}$	Vacuum residue	20
Eicosane	$C_{20}H_{42}$	Middle distillate	20
Heneicosane	$C_{21}H_{44}$	Lube oil light	10
Docosane	$C_{22}H_{46}$	Lube oil	10

The use of surrogate mixtures inevitably simplifies the true composition of refinery streams. In the present work, those fractions are represented by a reduced set of pseudocomponents chosen to reproduce the dominant thermophysical trends required for heat-transfer and exergy calculations rather than detailed compositional chemistry [25,48]. This level of representation is appropriate because the main objective of the study is to compare integration pathways under a consistent thermodynamic framework, not to reproduce refinery assay data at the molecular level.

Thermophysical properties were calculated using the `CoolProp` library with the same general assumptions introduced in Section 3. Enthalpy, entropy, density, and heat capacity were evaluated over the process-relevant temperature range for the surrogate mixtures and then used to construct the cumulative heat–temperature curves, entropy-generation integrals, and area calculations reported in the following subsections. A compact set of extended property data is retained in Appendix for traceability and reproducibility.

The representative-mixture approach has two practical advantages for the present study. First, it ensures internal consistency between the refinery heat-demand data summarized in Table 1 and the local thermodynamic models used in the heat-exchanger calculations. Second, it allows the interpretation of process-side irreversibilities to remain physically meaningful when comparing direct helium exchange with steam-mediated heat delivery. In other words, the refinery integration results below should be interpreted not as generic “crude heating” abstractions, but as calculations performed on thermodynamically defined surrogate streams representative of the Barrancabermeja case [6,19,28].

5.2. Direct helium coupling

Direct helium coupling represents the most immediate thermodynamic connection between the HTGR and the refinery process stream. In this configuration, reactor helium transfers heat directly to the crude feed entering the topping section, eliminating the intermediate steam loop and preserving the highest available temperature level from the reactor side. As such, this route defines the upper thermal potential of HTGR-based industrial heat integration, but also the most demanding condition in terms of heat-transfer matching, materials, and second-law performance [8,18].

For the refinery-side stream, the direct-helium topping case uses the representative light-to-medium mixture defined in Section 5.1 and Table 4. The thermodynamic properties of this surrogate stream were used to generate the cumulative heat–temperature curves and the second-law indicators discussed below, while extended property values remain available in Appendix.

Fig. 4 illustrates the direct coupling between the HTGR primary helium loop and the crude oil topping unit. In the consistent reference case used here, helium exits the reactor at 750 °C and transfers heat directly to the crude stream entering the distillation train.

The thermodynamic behavior of this configuration is governed by the large mismatch between the heat-capacity-flow characteristics of helium and the refinery hydrocarbon stream. As shown by the cumulative heat–temperature curves in Fig. 3, the hot and cold composite curves remain widely separated across most of the exchanger duty. The minimum temperature difference remains very large, and the heat-transfer process is characterized by steep local thermal gradients over a broad heat-load interval.

The operating conditions and mass-flow parameters adopted for this configuration are summarized in Table 6.

The performance indicators in Table 7 confirm that the resulting irreversibility is substantial. Entropy generation exceeds 200 kW/K, corresponding to an exergy destruction of nearly 64 MW, which is close to one quarter of the reactor thermal power. Under these conditions, direct helium coupling remains thermodynamically feasible, but its second-law performance is strongly penalized by the large temperature approach and by the inability to tune the helium-side effective heat-capacity flow independently of reactor design constraints [18,22,23].

From an engineering standpoint, this configuration should therefore be interpreted as a boundary comparison case rather than as the preferred near-term deployment route. Although direct helium transfer preserves the highest temperature level available from the reactor, it does so at the cost of severe thermal mismatch, high irreversibility, and stringent exchanger requirements. These characteristics explain why the direct route is useful as a thermodynamic benchmark, but not as the most practical refinery integration architecture.

5.3. Multi-stage process heating

To evaluate whether process-side heat cascading can improve the performance of direct helium coupling, a second configuration distributes reactor heat across two refinery duties: the topping and vacuum-heater sections. The purpose of this scenario is to test whether splitting the heat load across different process temperature levels can reduce the large thermal mismatch observed in the single-stage direct-helium case [25,28].

Table 6
Operating and thermodynamic parameters of the HTGR–topping furnace configuration with direct helium coupling, defining the heat duty, mass-flow rates, and boundary conditions governing temperature matching and irreversibility generation.

Characteristic	Value
Thermal power	250 MW_{th}
System configuration	Reactor – Topping
Coolant mass flow rate	96.35 kg/s
Secondary fluid mass flow rate	208 kg/s

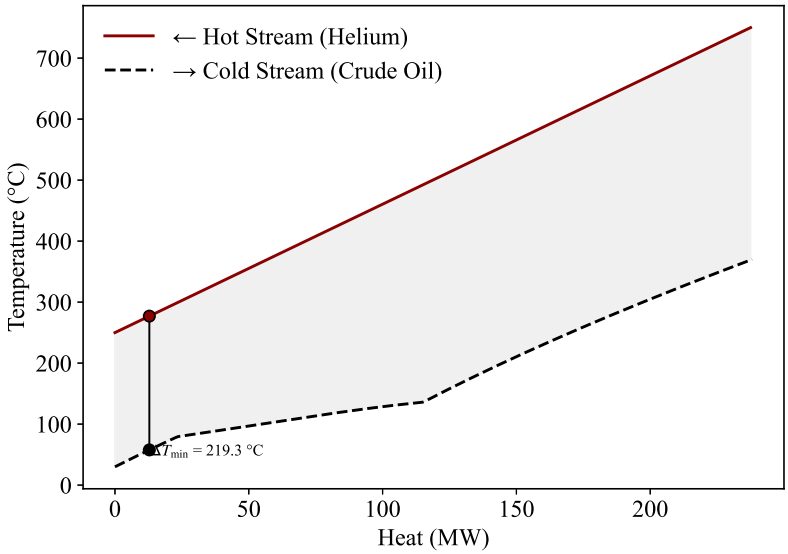

Fig. 3. Cumulative heat–temperature (CHT) curves for direct helium–crude oil heat exchange ($\varepsilon = 0.95$). The wide separation between hot and cold composite curves indicates strong thermal mismatch, resulting in large minimum temperature differences and high entropy generation.

Table 7
Heat-transfer and second-law performance indicators for the direct helium–crude oil topping exchanger. Large temperature differences drive high entropy generation and exergy destruction.

Parameter	Units	Value
Pinch-point temperature difference (ΔT_{min})	°C	219.3
Heat-transfer area (A)	m^2	2431.8
Entropy-generation rate ($\dot{S}_{gen}$)	kW/K	213.86
Exergy-destruction rate aprox. ($\dot{X}_{dest}$)	MW	63.76

In this configuration, the topping duty is represented by the light-to-medium mixture of Table 4, while the vacuum-heater duty is represented by the heavy surrogate mixture of Table 5. This allows the staged heating calculation to capture the different thermophysical responses of lighter and heavier refinery fractions without resorting to a fully assay-specific crude model. The supporting property basis for the heavier mixture is retained in Appendix.

Fig. 5 shows the corresponding cumulative heat–temperature behavior, while Table 8 summarizes the main operating conditions used in the multi-stage analysis. In this arrangement, helium from the reactor is used sequentially to supply the higher-temperature vacuum-heater duty and then the topping duty, thereby improving utilization of the reactor-side enthalpy drop.

The multi-stage arrangement produces a measurable but limited thermodynamic improvement. As the heat duty is distributed more effectively across the refinery temperature ladder, the entropy-generation rate decreases and exergy destruction is reduced relative to the single-stage direct-helium case, as quantified by the performance indicators in Table 9. This confirms that better use of reactor enthalpy is possible when multiple process sinks are arranged in series.

However, the improvement remains incremental rather than structural. The minimum temperature difference still exceeds 200 °C, indicating that the dominant source of irreversibility is not simply the lack of staging, but the intrinsic mismatch between helium and hydrocarbon process streams. Even with cascading, the direct-helium route retains high exergy losses and only a moderate gain in second-law efficiency [22,23,27].

This result is important for the logic of the paper because it shows that process rearrangement alone cannot overcome the thermodynamic limitation of direct helium coupling. Multi-stage heating improves reactor-side heat utilization, but it does not fundamentally change the quality of the thermal match. As a result, the direct-helium route remains better interpreted as a high-temperature comparison case than as the preferred industrial solution for refinery retrofits.

5.4. Steam-based OTSG integration

A fundamentally different integration pathway introduces an intermediate steam loop between the reactor and the refinery. In this configuration, helium first transfers heat to an OTSG, generating high-pressure steam that is subsequently supplied to the topping and

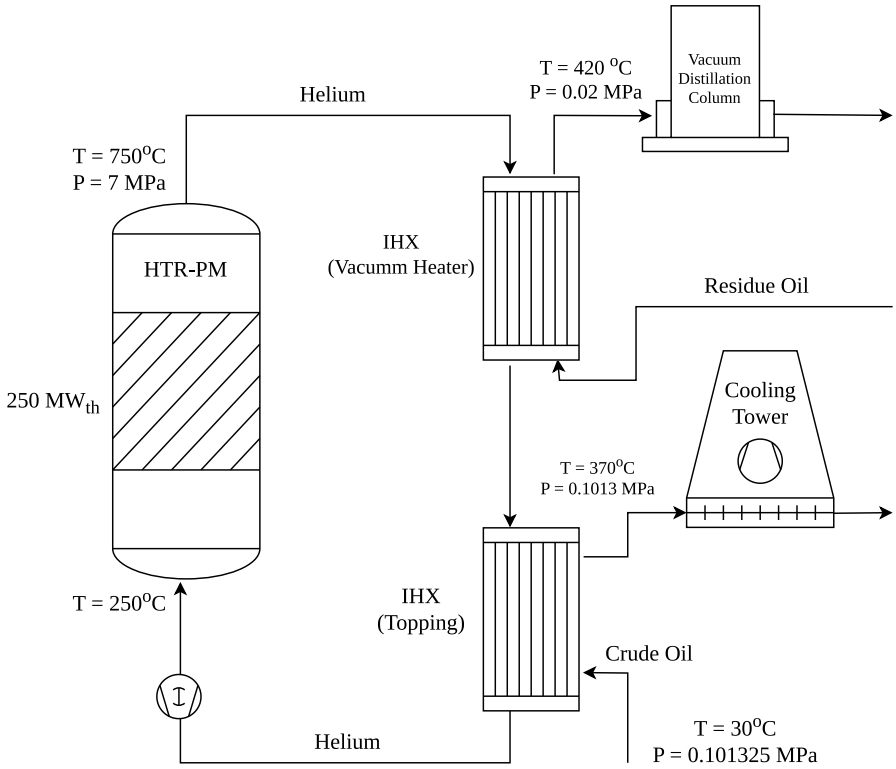

Fig. 4. Process-flow diagram of the direct HTGR–crude oil topping configuration, where high-temperature helium transfers heat directly to the crude stream. The large temperature gradients established across the exchanger define the dominant sources of entropy generation and exergy destruction in the second-law analysis.

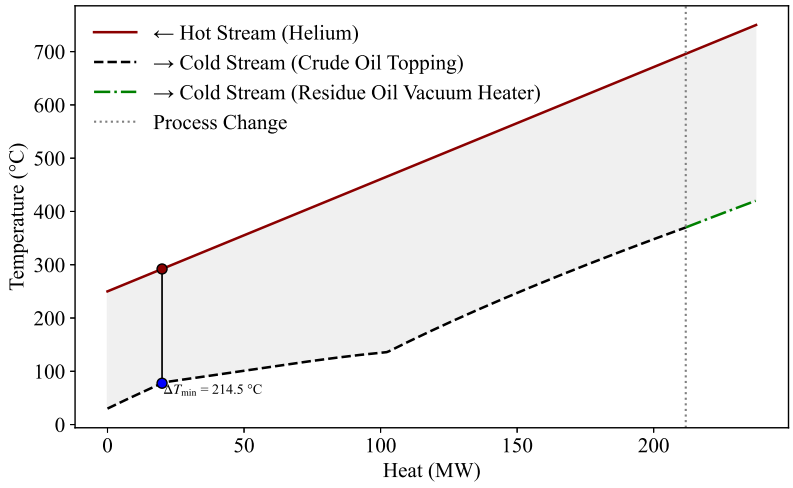

Fig. 5. Cumulative heat–temperature (CHT) curves for direct helium coupling to topping and vacuum-heater units (ε = 0.95). Partial heat cascading improves mid-range thermal matching, but large minimum temperature differences persist and limit exergy recovery.

Table 8
Thermodynamic configuration of the HTGR–refinery system with direct helium coupling to topping and vacuum-heater units, establishing the mass-flow distribution and thermal duties used in the multi-stage heat-exchange analysis.

Characteristic	Value
Thermal power	250 MW_{th}
System configuration	Reactor – Vacuum Heater – Topping
Coolant mass flow rate	96.35 kg/s
Crude oil mass flow rate	185 kg/s
Residue oil mass flow rate	165 kg/s

Table 9
Heat-transfer and second-law performance indicators for the direct helium multi-stage refinery configuration including vacuum-heater and topping duties.

Parameter	Units	Value
Pinch-point temperature difference (ΔT_{min})	°C	214.5
Heat-transfer area (A)	m^2	2735.90
Entropy-generation rate ($\dot{S}_{gen}$)	kW/K	188.44
Exergy-destruction rate aprox. ($\dot{X}_{dest}$)	MW	56.18

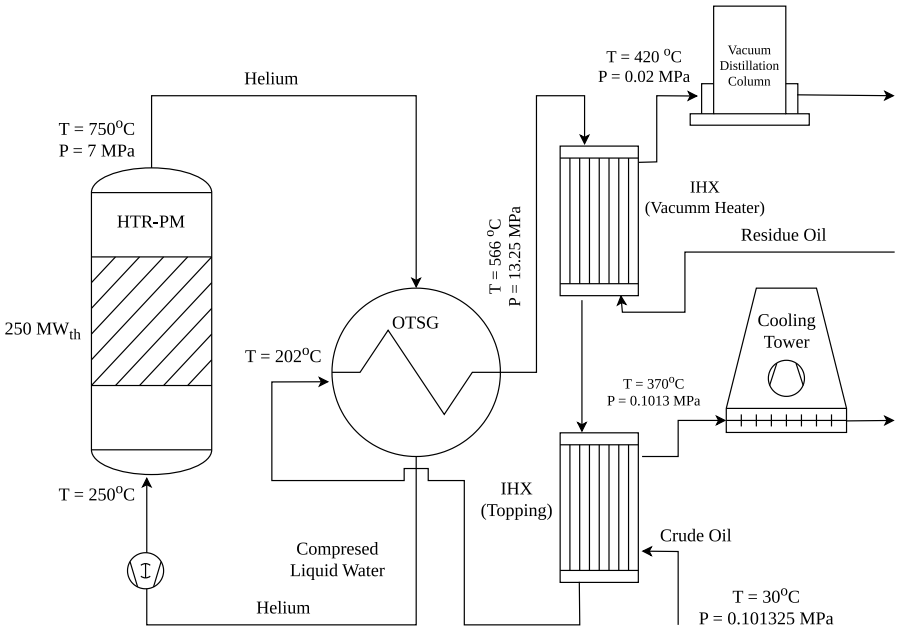

Fig. 6. Process-flow diagram of the HTGR–OTSG–refinery integration using an intermediate steam loop. The secondary steam circuit thermally decouples the nuclear and industrial systems while improving temperature matching and reducing irreversibility in downstream process heat exchangers.

Table 10
Thermodynamic configuration of the HTGR–steam–refinery system employing an OTSG, defining the operating conditions that enable improved thermal compatibility and reduced exergy destruction.

Characteristic	Value
Thermal power	250 MW_{th}
System configuration	Reactor – Steam – Refinery
Coolant mass flow rate	89.81 kg/s
Crude oil mass flow rate	168 kg/s
Residue oil mass flow rate	94 kg/s

vacuum-heater units through refinery-side heat exchangers and steam headers. This architecture is consistent with the component-level baseline established in Section 4 and with the reference reactor interfaces defined for the HTR-PM and Xe-100 [13,15,18].

The refinery-side exchangers in this configuration again use the representative mixtures introduced in Section 5.1: the light-to-medium mixture for topping service and the heavy mixture for the vacuum-heater service. Their use is particularly important in the steam-based configuration because the lower process-side temperature mismatch makes the local heat-capacity trajectory of the refinery stream more influential on the final values of ΔT_{min}, A, $\dot{S}_{gen}$, and $\dot{X}_{dest}$. Additional thermophysical data for the heavy mixture are reported in Appendix.

Fig. 6 illustrates the steam-based configuration, and Table 10 summarizes the corresponding operating conditions. Relative to direct helium coupling, the key thermodynamic advantage of this route is that the intermediate steam loop reshapes the temperature profile delivered to the refinery, producing a much better match with the process-side heat-demand trajectory.

The cumulative heat–temperature curves in Fig. 7 confirm the thermodynamic benefit of the steam route. The temperature gap between hot and cold composite curves is substantially compressed relative to the direct-helium cases, and the resulting heat-transfer path is much closer to near-isothermal behavior over the relevant duty range.

The performance indicators in Table 11 show that the reduction in irreversibility is decisive. Compared with direct helium coupling, the steam-based route cuts entropy generation by roughly half and reduces exergy destruction from about 60 MW to roughly 28–36 MW per 250 MW_{th} module, depending on the specific exchanger duty and interpretation basis. The corresponding second-law efficiency reaches approximately 89%, making this the best-performing configuration among all the refinery process-heat pathways evaluated in the present work [18,22,23].

Although the required heat-transfer area (4253.3 m^2) is larger than in the direct-helium case, this increase is not a disadvantage in system terms. Rather, it reflects the fact that the steam-based route exchanges heat with a much smaller temperature driving force and therefore with much lower exergy penalty. The resulting area requirement remains compatible with industrial-scale intermediate exchangers and is consistent with the role of the OTSG as an effective exergy-conditioning stage between the reactor and the refinery.

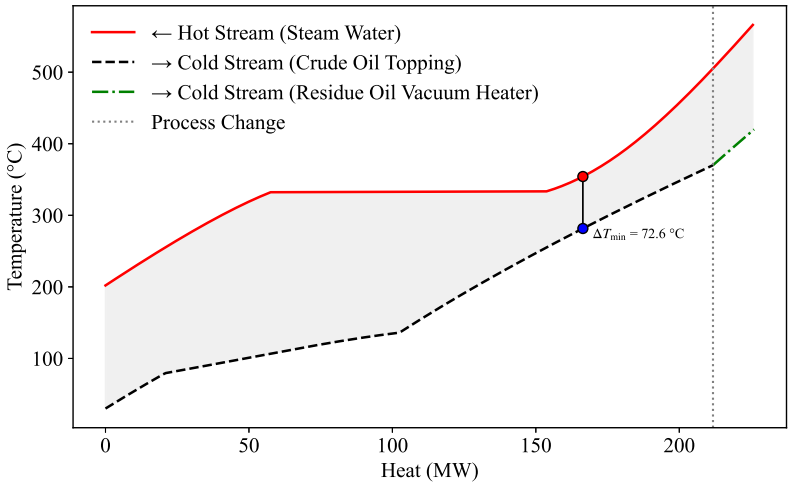

Fig. 7. Cumulative heat–temperature (CHT) curves for steam–crude oil heat exchange in topping and vacuum-heater units ($\varepsilon = 0.95$). The reduced temperature gradients indicate much better thermal matching and significantly lower entropy generation than in direct helium coupling.

Table 11
Heat-transfer and exergy-analysis parameters for steam–crude oil heat exchangers in topping and vacuum-heater units, demonstrating reduced entropy generation and substantially lower exergy destruction than in the direct helium configurations.

Parameter	Units	Value
Pinch-point temperature difference ($\Delta T_{\min}$)	°C	72.6
Heat-transfer area – Vacuum heater (A)	m²	4253.3
Entropy-generation rate ($\dot{S}_{\text{gen}}$)	kW/K	119.97
Exergy-destruction rate aprox. ($\dot{X}_{\text{dest}}$)	MW	35.77

The second-law efficiency of the heat transfer process was evaluated as

$$\eta_{II} = 1 - \frac{\dot{X}_{dest}}{\dot{X}_{in}} \tag{13}$$

where $\dot{X}_{dest}$ represents the exergy destruction associated with the irreversibilities of the heat-exchange process, and $\dot{X}_{in}$ corresponds to the exergy supplied by the hot stream [22,23].

For the helium-based configurations, the exergy supplied by the hot stream was estimated using the analytical expression for an ideal gas with approximately constant specific heat:

$$\dot{X}_{in} \approx \dot{m} c_p \left[(T_{in} - T_{out}) - T_0 \ln \left(\frac{T_{in}}{T_{out}} \right) \right] \tag{14}$$

which provides a consistent approximation for comparative second-law assessment under the reactor-side conditions considered in this work [22,51].

For the steam-based configuration, the exergy supplied by the hot stream was calculated using the physical exergy formulation based on real fluid properties:

$$\dot{X}_{in} = \dot{m} \left[(h_{in} - h_{out}) - T_0 (s_{in} - s_{out}) \right] \tag{15}$$

where h and s represent the specific enthalpy and entropy of the steam stream at the inlet and outlet of the heat exchanger, respectively, and T_0 is the ambient temperature.

This formulation accounts for the non-ideal thermodynamic behavior of water at high pressure and temperature and therefore provides a more accurate evaluation of the exergy supplied by the steam stream.

It should be noted that, in the steam-based configuration, an additional source of irreversibility must be considered. Prior to process heat utilization, thermal energy from the helium coolant is first transferred to water in the OTSG. This intermediate heat transfer process introduces additional entropy generation and therefore additional exergy destruction; this was quantified in Table 12.

Taken together, the refinery-side results show that the intermediate steam loop is not simply a compromise imposed by safety and engineering practice. It is also the thermodynamically preferred architecture for transferring HTGR heat to refinery streams whose temperature trajectories are poorly matched to direct helium cooling. This observation is the central result of the present section and provides the basis for the deployment interpretation developed next (see Table 13).

6. Hydrogen production and cogeneration

The results of Section 5 show that, after the main refinery process-heating duties have been supplied, a significant fraction of high-quality thermal exergy remains available from the HTGR system. Rather than dissipating this potential through single-purpose heat rejection, it can be redirected toward additional refinery services that make better use of the reactor's temperature and exergy levels.

This section examines three complementary extensions of the refinery integration framework. First, high-temperature nuclear hydrogen pathways are framed, with HTSE adopted as the principal fully nuclear route evaluated in detail. Second, nuclear-assisted steam methane reforming (SMR-H_2) preheating is discussed as a transitional option that can reduce emissions while preserving compatibility with existing refinery assets. Third, Rankine- and Brayton-based cogeneration schemes are considered to illustrate how HTGR output can be distributed among process heat, hydrogen production, and electricity generation within an integrated industrial energy system.

6.1. High-temperature hydrogen pathways for refineries

Hydrogen is a strategic component of refinery decarbonization because it is a core input for hydrotreating, hydrocracking, and deep desulfurization. This is particularly important for the Barrancabermeja Refinery, where hydrogen demand is large enough that decarbonizing process heat alone would still leave a substantial share of fossil-derived

Table 12
Comparative summary of thermodynamic performance indicators for the evaluated HTGR–refinery integration configurations.

Configuration	$\dot{S}_{gen}$ (kW/K)	$\dot{X}_{dest}$ (MW)	η_{II} (%)
Direct helium (Topping)	213.86	63.76	57.50
Direct helium (Vacuum + Topping)	188.44	56.18	62.54

Table 13
Second-law performance of the steam-mediated heat integration configuration.

Configuration	$\dot{S}_{gen}$ (kW/K)	$\dot{X}_{dest}$ (MW)	$\eta_{II_{OTSG}}$ (%)	η_{II_R} (%)
Steam-based (OTSG coupling)	119.97	35.77	70.66	62.46

emissions associated with upgrading operations. In this context, hydrogen should be treated as part of the same integrated energy system as process heat rather than as an independent downstream utility.

HTGRs are especially well suited for low-carbon hydrogen production because they can support both high-temperature steam electrolysis (HTSE) and thermochemical pathways such as sulfur–iodine (S–I), hybrid sulfur (HyS), hydrogen–bromine (H–Br), and other high-temperature water-splitting configurations. Their ability to provide stable heat in the approximate 750–950 °C range allows a significant fraction of the process energy demand to be supplied directly as heat, reducing the electrical burden relative to low-temperature electrolysis and improving the overall utilization of reactor exergy [8,35,52]. Previous HTGR–SOEC coupling studies have reported thermal-to-hydrogen efficiencies on the order of 45%–50%, confirming the thermodynamic advantage of combining high-temperature reactors with advanced hydrogen production routes [8,53].

Within this broader framework, HTSE is the most direct option for integration with the steam-based heat-delivery architecture developed in Section 5.3, since the remaining high-quality exergy of the reactor can be redirected to solid oxide electrolysis once medium-grade refinery heat has already been extracted. Thermochemical cycles, however, should not be interpreted as marginal alternatives. They belong to the same high-temperature hydrogen landscape and may become especially attractive when the objective is to maximize direct thermal utilization rather than rely primarily on electricity. In that sense, HTSE and thermochemical cycles are better understood as complementary pathways within a broader HTGR-based hydrogen portfolio.

This broader perspective is reinforced in the Colombian context by the recent study of Gómez Carvajal et al. [54], who evaluated HTGR-based hydrogen production using HTSE together with four thermochemical routes: S–I, HyS, H–Br, and Mg–Cl. For a modular HTGR system composed of eight 125 MWe units, they report maximum annual hydrogen productions of 203.5 kt/year for HTSE, 70.8 kt/year for S–I, 166.5 kt/year for HyS, 148.0 kt/year for H–Br, and 277.5 kt/year for Mg–Cl, with corresponding hydrogen-plant efficiencies of 40.6%, 26.98%, 61.03%, 47.55%, and 44.63%, respectively [54]. These results show that HTSE combines high output with direct compatibility with steam-based HTGR integration, while some thermochemical routes can achieve either higher conversion efficiency or greater hydrogen yield under favorable conditions [54].

For Barrancabermeja, whose hydrogen demand can be estimated at approximately 114 t/day (~41.6 kt/year) based on Ecopetrol's reported refining-system hydrogen consumption and the share attributed to the Barrancabermeja site [55], even the lowest-output route reported by Gómez Carvajal et al. would nominally cover the refinery's current annual requirement [54,55]. This suggests that the key issue is not production sufficiency, but the thermodynamic and strategic choice of pathway within a broader allocation of reactor exergy between process heat, electricity, and hydrogen. Within that framework, HTSE remains the most coherent fully nuclear option for the present study, whereas the thermochemical routes define the wider long-term performance envelope of HTGR-based hydrogen supply [8,54].

6.2. Hybrid HTGR–SMR-H_2 preheating

While Section 6.1 framed HTSE as the principal long-term fully nuclear pathway for refinery hydrogen supply, existing refineries are unlikely to replace steam methane reforming assets immediately. This is particularly true for brownfield sites such as Barrancabermeja, where hydrogen is already produced through fossil-based reforming units embedded in the broader refinery utility system. A more immediate transition route therefore consists of using HTGR heat to preheat the steam–methane feed mixture upstream of the reformer while preserving the catalytic reforming section, shift conversion, and downstream purification train. In this hybrid arrangement, nuclear heat does not eliminate SMR-H_2 as a process, but reduces the fossil firing duty required to bring the feed to full reforming conditions.

Fig. 8 presents the cumulative heat–temperature behavior for helium–steam–methane heat exchange in this preheating configuration. The pinch point appears near the hot end of the exchanger, showing that the same thermodynamic limitation identified in the refinery direct-helium cases also emerges here: as the cold stream approaches the high temperatures required for reforming, the local temperature driving force collapses and the exchanger becomes increasingly constrained. This confirms that direct helium transfer is poorly matched to the final high-temperature segment of a strongly endothermic reforming duty, even when it remains useful for upstream sensible heating.

The thermodynamic implication is therefore specific and practically important. Under optimistic exchanger assumptions, the HTGR helium stream can raise the reformer feed only to approximately 720–740 °C, which remains below the preferred reforming range of about 800–950 °C for conventional nickel-catalyzed steam methane reforming. Direct helium heating is thus not sufficient, by itself, to sustain the full reforming reaction zone. However, this does not diminish the value of the concept; rather, it defines its proper role. Nuclear heat is most effective here as a preheating stage that displaces a substantial fraction of the sensible-heating burden otherwise supplied by the reformer furnace, while the residual high-temperature duty remains concentrated in the catalytic section. This interpretation is consistent with previous studies of HTGR-assisted reforming, which likewise conclude that nuclear heat is best used to offset upstream furnace duty rather than to replace the entire endothermic reforming train [56,57].

For Barrancabermeja, this pathway is especially relevant because the refinery already operates fossil-based hydrogen production units and faces decarbonization pressure without the practical possibility of instantaneous process substitution. In that context, hybrid preheating offers a retrofit-compatible route that preserves the installed reformer asset base while reducing natural-gas combustion and associated emissions. Based on the heat-transfer behavior obtained here, helium preheating could reduce auxiliary firing requirements by roughly 25%–35%, depending on feed conditions, heat allocation, and reformer operation. Since hydrogen production constitutes a significant share of the refinery's fossil energy use, this partial substitution can produce meaningful CO_2 abatement while avoiding the institutional and capital barriers associated with immediate full replacement of SMR-H_2 units.

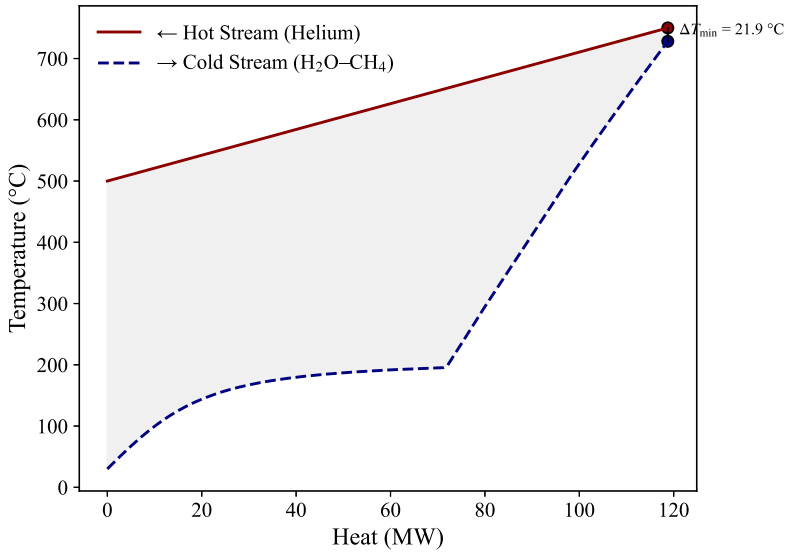

Fig. 8. Cumulative heat–temperature (CHT) curves are presented for the counter-current heat exchange between helium and a steam–methane mixture with a molar ratio of 3:1. The mixture is preheated from 30 °C at a pressure of 2 MPa, assuming a heat exchanger (effectiveness of $\varepsilon = 0.95$) The pinch point is located near the hot end of the exchanger, limiting the maximum attainable preheating temperature. This behavior highlights the inherent thermodynamic constraint of direct helium coupling when supplying heat for fully endothermic steam reforming reactions.

Table 14
Comparison of conventional, hybrid, and fully nuclear hydrogen production pathways, highlighting temperature range, specific CO_2 emissions, and technology readiness.

Configuration	Effective process temperature (°C)	Specific CO_2 (kg CO_2/kg H_2)	TRL
Conventional SMR-H_2	800–950	8–10	9
HTGR + SMR-H_2 preheat (hybrid)	720–740 (He preheat)	5–7	6–7
HTGR + HTSE (fully nuclear)	750–950	< 1	5–6

This transitional role distinguishes the hybrid pathway from the fully nuclear logic of Section 6.1. HTSE represents the long-term route for deep refinery hydrogen decarbonization, whereas hybrid preheating is a brownfield integration strategy designed to operate within the constraints of current refinery hardware. Its value lies less in achieving minimum theoretical emissions than in providing an implementable intermediate step between conventional reforming and future fully nuclear hydrogen systems. In this sense, the hybrid option should be interpreted not as a competing endpoint, but as a deployment bridge that can accelerate emissions reductions before full HTSE deployment becomes technically and economically mature at refinery scale.

This interpretation is also consistent with the emerging literature on hybrid nuclear hydrogen systems. Yoo et al. [58], for example, analyzed a configuration combining HTGR heat, high-temperature electrolysis, and methane reforming for the simultaneous production of pink and grey hydrogen, showing that hybrid pathways can improve system economics during the transition toward fully nuclear hydrogen supply. Although their process layout differs from the refinery preheating configuration evaluated here, the broader lesson remains applicable: partial nuclear integration can play an important intermediate role when existing reforming infrastructure, capital stock, and staged decarbonization objectives must all be considered simultaneously.

Table 14 compares the three refinery-relevant deployment pathways examined quantitatively in this study: conventional SMR-H_2, hybrid HTGR–SMR-H_2 preheating, and HTGR–HTSE. The comparison should not be read as a binary competition between technologies, but as a staged deployment sequence for refinery decarbonization. Conventional reforming is the incumbent route, hybrid preheating is the retrofit transition step, and HTSE represents the long-term low-carbon option once broader nuclear–hydrogen integration becomes feasible.

From a systems perspective, the hybrid pathway reinforces one of the central conclusions of the present work: direct helium heat transfer is not best interpreted as the sole heat source for strongly mismatched industrial duties, but it can be highly effective when used selectively as a high-temperature preheater inside a broader cascaded architecture. For refinery hydrogen systems, this makes hybrid HTGR–SMR-H_2 preheating a technically meaningful and strategically credible transition route, especially in large brownfield sites such as Barrancabermeja, where phased decarbonization is more realistic than immediate technology replacement.

6.3. Rankine and Brayton cogeneration options

Beyond process heat and hydrogen production, HTGRs can also provide electricity and recoverable thermal energy through conventional power-conversion cycles. This capability is particularly relevant, as refinery decarbonization involves not only replacing fired heaters but also optimally allocating reactor thermal output among steam, electricity, and chemical energy pathways. Cogeneration therefore provides the system-level context within which the refinery integration scenarios discussed in Sections 5 and 6.1–6.2 should be interpreted.

The first representative configuration is a steam Rankine cycle with process steam extraction (Fig. 9). Reactor heat is transferred through an IHX and a OTSG to drive a steam turbine, where a controlled fraction of high-pressure steam is extracted for industrial use while the remaining flow generates electricity. This configuration benefits from high technological maturity and direct compatibility with existing refinery steam networks, making it suitable for near-term deployment.

The second configuration is a closed Brayton cycle with intermediate heat recovery (Fig. 10). In this case, thermal energy is extracted downstream of turbine expansion, where exhaust temperatures remain sufficiently high for direct process heat supply or secondary steam generation. From a second-law perspective, this approach preserves

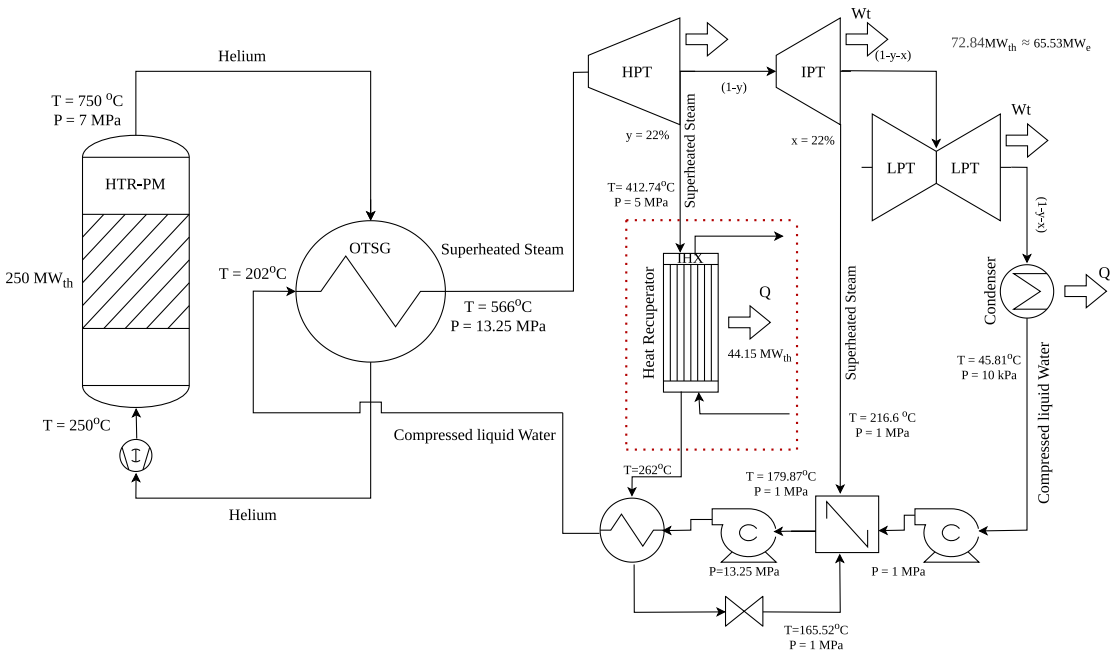

Fig. 9. HTGR–Rankine cogeneration scheme with steam extraction for process heat supply, illustrating the trade-off between electricity generation and exergy degradation.

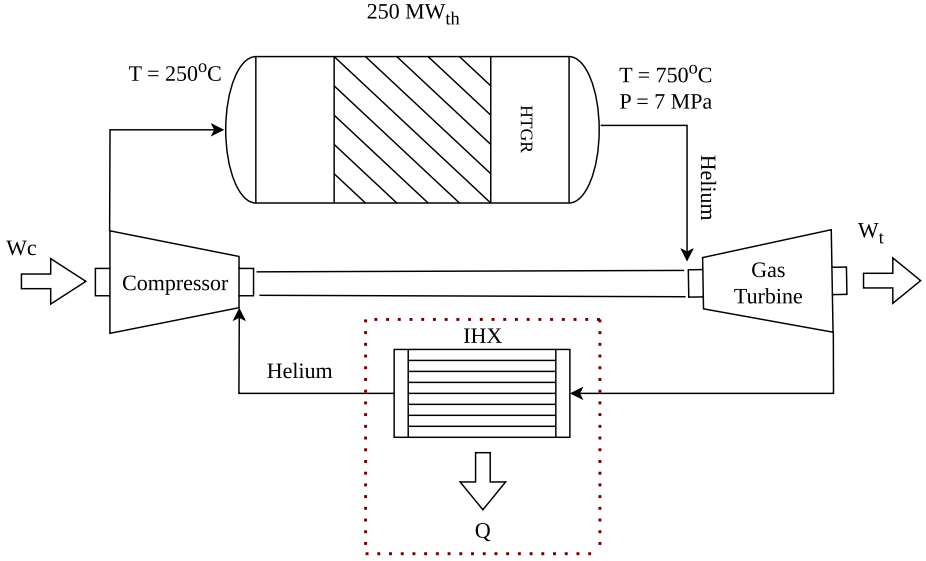

Fig. 10. Closed Brayton cycle coupled to an HTGR with intermediate heat recovery, enabling higher-temperature heat utilization and reduced exergy losses.

a larger fraction of high-temperature exergy than Rankine extraction, as heat recovery occurs at higher temperature levels. However, its implementation remains more challenging due to material constraints, leakage control, and turbomachinery requirements.

Table 15 summarizes representative operating conditions and recoverable energy levels for the evaluated waste heat recovery configurations. Rankine-cycle systems provide a balanced trade-off between net electrical output and moderate heat extraction, whereas Brayton-cycle configurations deliver significantly higher recoverable thermal power owing to their elevated post-expansion exhaust temperatures. The column *Energy* (MWe/year) represents the annual electrical generation potential under the combined operating conditions of net power output and thermal heat extraction, assuming a capacity factor of 92.75% [10]. Consequently, Brayton cycles are more suitable for high-temperature process integration or hydrogen production, while Rankine systems remain the most practical option for near-term refinery applications.

To retain a deployment-oriented perspective, Table 16 provides a qualitative comparison of the main hydrogen and cogeneration pathways. Rather than a detailed techno-economic assessment, it highlights relative maturity, integration complexity, and deployment timelines.

In the Rankine cycle, steam extraction levels remain relatively stable, but decreasing steam temperatures reduce the available exergy, limiting its use for high-grade applications. In contrast, Brayton cycles enable more efficient thermal utilization by maintaining higher temperature levels, allowing simultaneous electricity generation and high-quality heat recovery.

Table 15
Estimated operating conditions, generated power, and recoverable thermal energy for Rankine and Brayton cogeneration configurations.

Cycle	Configuration/ Key parameter	Operating range	Power (MW_e)	Heat (MW_{th})	Energy (MWh_e/year)
Rankine (extraction)	$y = 22\%$, 3 MPa	344.13 °C $T_{in} = 233.52$ °C	67.78	41.40	550.60
Rankine (extraction)	$y = 22\%$, 5 MPa	412.74 °C $T_{in} = 262$ °C	65.54	41.15	532.50
Rankine (extraction)	$y = 22\%$, 8 MPa	482.82 °C $T_{in} = 262$ °C	63.19	43.71	513.40
Brayton (closed)	PR = 2	528 °C $T_{comp} = 113$ °C	38.48	207.44	312.70
Brayton (closed)	PR = 4	359.82 °C $T_{comp} = 15$ °C	69.69	172.53	566.20

Table 16
Representative Max Steam production potential and energetic cost indicators.

Method	Max Steam (kg/s)	P (MPa)	T (°C)	Electrical impact	Thermal cost (MW_{th})
OTSG	89.81	13.25	566	–	2.64
IHX after GT (Brayton)	50	5	450	None	3.23
IHX after GT (Brayton)	70	3	260	None	2.80
Rankine extraction (8 MPa)	19.75	8	482	Penalty	≈0.38
Rankine extraction (5 MPa)	19.75	5	412	Penalty	≈0.31
Rankine extraction (3 MPa)	19.75	3	348	Penalty	≈0.24

The simplified configurations analyzed prioritize thermal energy recovery, enabling a first-order assessment of their feasibility for refinery integration. For a representative 100 kbpd refinery, steam demand is approximately 39 MW_{th} and 28 MW_{th} [59]. Industrial requirements typically involve high-pressure (~5 3 MPa) and low-pressure (~1 –0.3 MPa) steam, representing 30%–60% of total demand within a temperature range of 141–350 °C [59].

For the Barrancabermeja refinery, estimated demands reach 89.7 MW_{th} and 64.4 MW_{th}, underscoring the relevance of these configurations for large-scale integration [6,19].

In Table 16, the *penalty* denotes the reduction in net power output resulting from steam extraction. The *thermal cost* represents the thermal energy consumed in steam production that is permanently removed from the energy conversion chain; since the extracted auxiliary steam does not recirculate, each unit of thermal energy diverted cannot be recovered for further electrical generation or cogeneration purposes. In other words, the thermal cost quantifies the irreversible thermal expenditure, expressed in MWth, associated with producing each megawatt of extracted steam under the specified operating conditions.

These conditions are consistent with typical refinery steam headers and are suitable for common operations such as distillation, stripping, and process heating. The configurations considered are directly derived from the system layouts presented in this work, where steam generation is achieved through IHX–OTSG coupling.

From a system perspective, these options should be interpreted as complementary modes of exergy allocation rather than competing alternatives. A rational strategy prioritizes process heat supply, followed by hydrogen production, and finally electricity generation from residual thermal energy.

This hierarchy is consistent with previous studies on HTGR integration with thermochemical cycles, solid oxide electrolysis, and industrial processes [52,60–62]. These works support the interpretation of HTGRs as high-temperature energy hubs rather than purely electricity-generating systems.

Overall, OTSG-based integration remains the most practical near-term solution for refinery heat supply, HTSE defines a coherent long-term pathway for hydrogen production, and hybrid HTGR–SMR preheating offers a viable transition strategy. Within this framework, Rankine and Brayton cycles enable flexible cogeneration, allowing process heat, electricity, and chemical energy to be allocated according to thermodynamic quality.

7. Integrated deployment architecture for the Barrancabermeja refinery

The results of Sections 5 and 6 define a refinery-scale deployment architecture for the Barrancabermeja Refinery. The central result is that the thermodynamic advantage of the OTSG-based configuration extends beyond individual exchanger performance and remains valid at system scale. The preferred architecture is therefore not the one that preserves the highest temperature at the process boundary, but the one that minimizes irreversibility across the full heat-delivery chain.

Fig. 11 summarizes this system-level interpretation. It should be read as an integrated deployment concept in which reactor output is distributed according to the exergy hierarchy identified in the preceding sections. High-grade nuclear heat is first conditioned through the OTSG and then assigned to the refinery duties with the highest temperature requirements, while the remaining thermal potential is directed to the steam network, cogeneration, and hydrogen-related services.

Under this interpretation, the integrated system recovers approximately 419 MW_{th} through process heat exchangers, generates about 27 kg/s of low-pressure steam and 7 kg/s of high-pressure steam, and retains a net electrical output of approximately 14.45 MW_e. The corresponding throughput is about 200 kbpd. The figure should therefore be interpreted as a physically grounded integration proposal derived from the thermodynamic results, rather than as a definitive plant layout.

This architecture also implies a multi-module deployment strategy. The Barrancabermeja process-heat demand lies in the several-hundred-megawatt range, making clustered HTGR deployment the most realistic route for displacing the most carbon-intensive fired-heater duties while preserving flexibility for hydrogen production and cogeneration. For the HTR-PM, this corresponds to about three 250 MW_{th} modules; an equivalent Xe-100 deployment would require a larger number of 200 MW_{th} modules, although the thermodynamic basis would remain unchanged because the system-level benefit arises primarily from steam-mediated heat delivery rather than reactor design alone.

The practical relevance of this interpretation is reinforced by the compatibility assessment in Table 17. Most major Barrancabermeja process units are thermodynamically compatible with HTGR-based heat supply, particularly through the OTSG steam route. In this table, *Feasible* denotes thermodynamic compatibility with the temperature and interface conditions of the process unit, whereas *Partial* indicates that

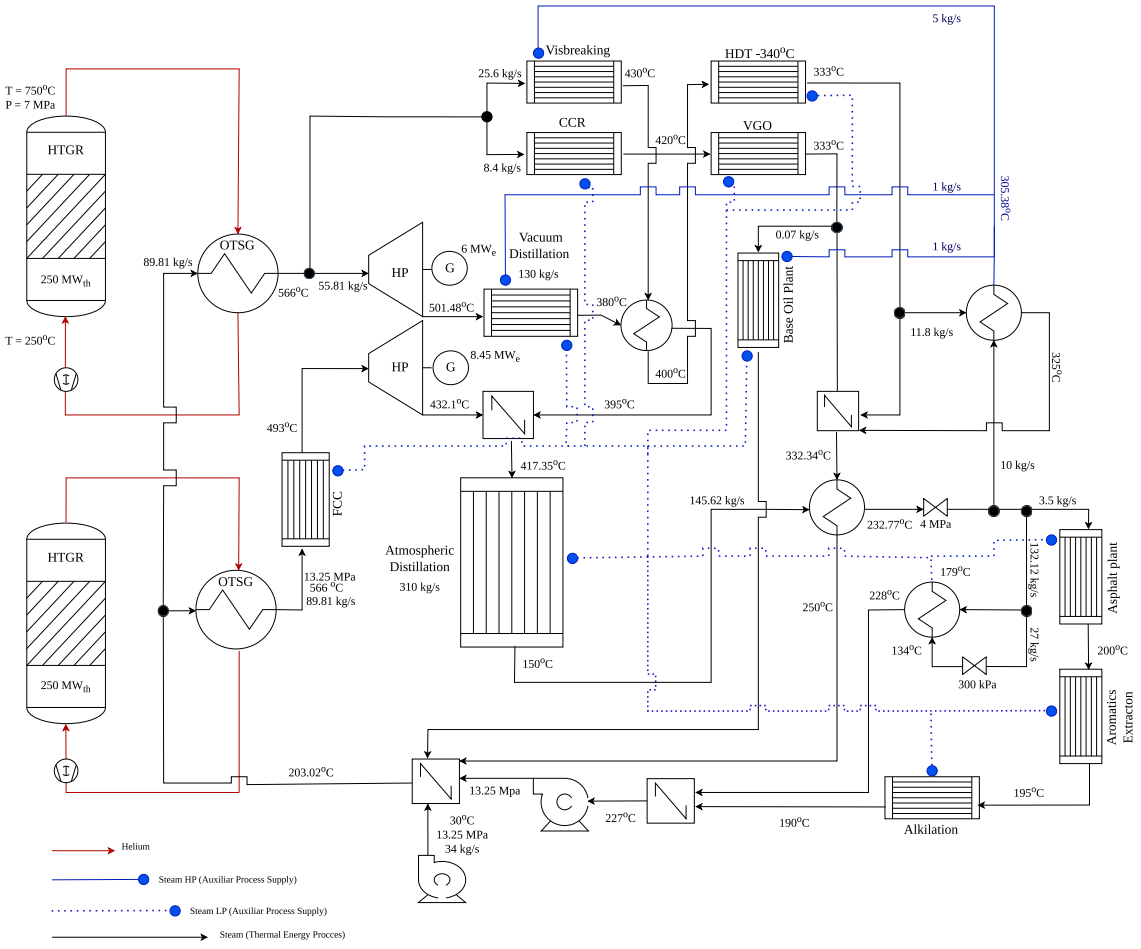

Fig. 11. Thermodynamic process diagram illustrating a modular HTGR-based integration concept for a refinery system with process units, heat duties, and steam demand equivalent to those of the Barrancabermeja refinery. The configuration incorporates high-temperature heat supply, multi-pressure steam networks, and cogeneration pathways, assuming $\eta_{turb} = \eta_{gen} = 0.90$ and $\epsilon = 0.95$ for heat exchangers.

Table 17
Compatibility of HTGR-based heat-delivery configurations with major refinery processes based on temperature requirements and interface conditions. For hydrogen pathways, the classification refers only to direct process-heat delivery to the corresponding unit and does not represent an assessment of the overall feasibility of nuclear-assisted hydrogen production.

Process unit (Temperature range)	Direct helium	OTSG steam	Brayton	Rankine
Atmospheric distillation (350–380 °C)	Feasible	Feasible	Feasible	Partial
Vacuum distillation (380–430 °C)	Feasible	Feasible	Feasible	Partial
FCC feed preheating (450–520 °C)	Feasible	Feasible	Partial	Not feasible
Visbreaking (450–480 °C)	Feasible	Feasible	Partial	Not feasible
CCR reforming (450–520 °C)	Feasible	Feasible	Partial	Not feasible
HDT heaters (320–370 °C)	Feasible	Feasible	Feasible	Partial
VGO hydrotreating (340–380 °C)	Feasible	Feasible	Feasible	Partial
FCC naphtha hydrotreating (250–350 °C)	Feasible	Feasible	Feasible	Feasible
Base oil and asphalt (200–300 °C)	Feasible	Feasible	Feasible	Feasible
SMR-H_2 (30–950 °C)	Feasible (only preheat)	Not feasible for direct unit heat delivery	Not feasible	Not feasible
HTSE (30–950 °C)	Feasible (only preheat)	Not feasible for direct unit heat delivery	Not feasible	Not feasible

Table 18
Technological Readiness Level (TRL) assessment of HTGR-based heat-delivery configurations.

Configuration	TRL	Justification
Direct helium (He–crude)	3–4	Conceptual stage with no demonstrated helium–crude heat exchangers; limited to analytical and experimental studies.
Helium–OTSG–crude	9	High maturity due to proven IHX technology and widespread industrial use of steam-based heat exchange systems.
Rankine integration	9	Fully mature technology with extensive industrial and nuclear deployment of steam turbines and associated systems.
Brayton integration	4	Limited to conceptual and pilot-scale developments; no industrial helium turbine systems for refinery heat applications.

the duty can only be met under restricted operating conditions or with additional integration measures.

The same conclusion is supported by the technology-readiness assessment in Table 18. The helium–OTSG–crude pathway is not only the thermodynamically referred option, but also the most credible near-term route for implementation. By contrast, direct helium-to-crude integration remains useful as an upper-temperature benchmark, yet significantly less mature as an industrial deployment pathway.

Within this refinery-scale framework, hydrogen production is best interpreted as an additional outlet for preserved high-grade exergy rather than as a separate subsystem. HTSE represents the most coherent long-term fully nuclear pathway, whereas hybrid nuclear preheating of SMR-H_2 feedstock defines a more immediate transition route for existing refinery assets. The deployment logic is therefore common across process heat, hydrogen, and cogeneration: high-quality thermal resources should be allocated first to the most temperature-demanding services and only then to lower-grade uses.

This same logic clarifies the role of modularity. The configuration shown in Fig. 11 is best understood as an initial deployment case that illustrates the thermodynamic structure of the concept. Full coverage of the principal refinery thermal demand would require the addition of a third HTGR module. This staged interpretation is fully consistent with the modular character of HTGR deployment, in which capacity can be added progressively as process-heat, hydrogen, and steam-network demands are incorporated.

Fig. 12 extends this interpretation by showing how additional HTGR modules can increase refinery heat coverage and strengthen hydrogen-related services within the same thermodynamic framework. As helium–steam heat exchange and associated integration pathways move closer to commercial deployment, modularity becomes more than a reactor attribute; it becomes the basis for phased refinery decarbonization. In that sense, the OTSG-based architecture should be understood as the thermodynamic backbone of HTGR-assisted refinery decarbonization because it combines temperature compatibility, exergy preservation, and technology readiness more effectively than the direct-helium alternatives.

8. Conclusions

This study examined how HTGR–SMRs can be coupled to refinery process heat, hydrogen production, and cogeneration under realistic thermodynamic constraints, using the Barrancabermeja Refinery as the reference case.

The results show that the central integration problem is not the availability of high temperature, but the thermodynamic quality of the reactor–process match and the way high-grade heat is allocated across refinery services. At the component level, the helium–water OTSG provides an effective intermediate interface, with a minimum temperature difference of 39.3 °C, a heat-transfer area of 3119.6 m^2, and an exergy-destruction rate of 15.59 MW. At the refinery level, indirect steam delivery through the OTSG and direct helium supply to multiple process duties achieve comparable second-law performance, with efficiencies of about 62.46–62.54%, whereas direct helium coupling to the topping unit alone performs less favorably, with a second-law efficiency of 57.50% and an exergy-destruction rate of 63.76 MW. These results confirm that the observed thermodynamic differences do not arise from the OTSG itself, but from the degree of thermal matching between the heat source and the refinery duties.

From this perspective, the OTSG-based route remains the most credible near-term configuration for refinery integration, not because it inherently eliminates irreversibilities, but because it enables a more effective redistribution of heat quality across the refinery network while preserving hydraulic and operational separation between the nuclear and industrial systems. The staged direct-helium case reduces exergy destruction relative to topping-only heating, but still remains constrained by the intrinsic mismatch between helium cooling and hydrocarbon heating trajectories.

The hydrogen and cogeneration results support the same system-level interpretation. HTSE remains the most coherent long-term pathway for fully nuclear low-carbon hydrogen production, whereas nuclear-assisted SMR-H_2 preheating provides a practical transition option for existing refinery assets. More broadly, the results indicate that HTGRs should be interpreted not simply as substitutes for fired heaters, but as integrated energy platforms capable of allocating heat, steam, electricity, and hydrogen according to exergy quality.

In terms of deployment, the energy balances reported in this work correspond specifically to the configurations presented Figs. 11 and 12. For the two-reactor configuration shown in Fig. 11, the system uses approximately 419 MW_{th} in process heat exchange and auxiliary steam generation, while also producing 14.45 MW_e, corresponding to a refinery processing capacity of about 200 kbpd. Under this configuration, the electrical efficiency is about 2.9%, while the overall energy efficiency reaches 86.7%, indicating that most of the nuclear output is effectively directed to process applications rather than electricity generation.

If a third 250 MW_{th} module is incorporated under the configuration represented in Fig. 12, approximately 118.75 MW_{th} from helium cooling could be used for preheating the natural gas–steam mixture in the SMR-H_2 process, while an additional 118.75 MW_{th} would remain available for other refinery duties, electricity generation, or related services. In this sense, three 250 MW_{th} HTR-PM modules, or an equivalent Xe-100 multi-module deployment, define a realistic modular pathway toward supplying about 400 MW_{th} of refinery process heat while preserving flexibility for hydrogen and cogeneration integration.

From a climate perspective, this integration framework suggests a technically structured pathway for deep refinery decarbonization in large industrial sites with multi-vector energy demand. For Barrancabermeja, the manuscript indicates that HTGR integration at this scale could avoid on the order of 3 Mt CO_2/year while replacing a substantial share of fossil-fired process heat and enabling lower-carbon hydrogen pathways.

The present work remains a thermodynamic feasibility and architecture study rather than a final engineering design. The analysis assumes steady-state operation, representative surrogate mixtures, and simplified exchanger and integration conditions. Future work should extend the framework toward dynamic operation, detailed balance-of-plant design, site-specific techno-economic assessment, and regulatory evaluation of coupled nuclear–industrial systems.

The main contribution of this work is to provide a unified second-law basis for comparing HTGR–refinery coupling pathways and to show

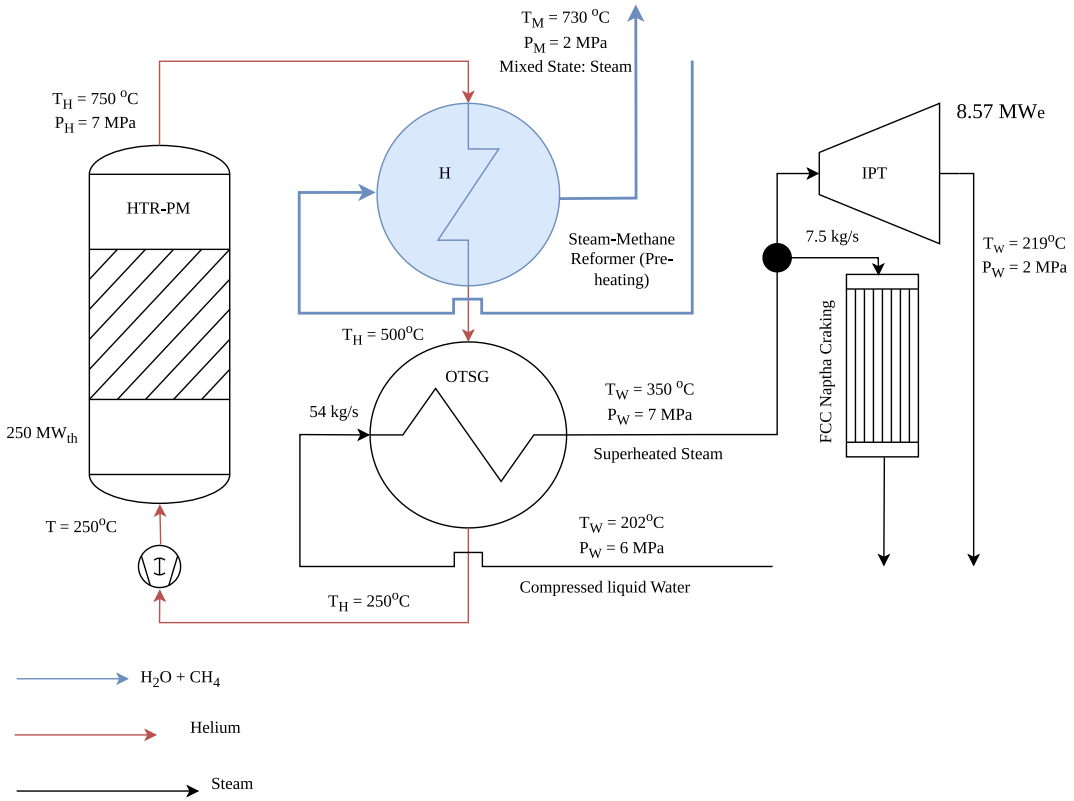

Fig. 12. Conceptual modular HTGR–H_2–OTSG configuration illustrating the potential integration of multiple HTGR modules to supply both thermal and electrical energy, enabling broader demand coverage of the Barrancabermeja refinery.

that the thermodynamic benefit of OTSG-centered integration arises primarily from improved heat allocation and thermal matching across refinery services, rather than from the intermediate steam loop alone.

CRediT authorship contribution statement

Nicolas Enciso: Conceptualization, Methodology, Investigation, Data curation, Writing – original draft, Writing – review & editing. **Daniel Morales:** Conceptualization, Methodology, Investigation, Data curation, Writing – original draft, Writing – review & editing.

Declaration of Generative AI and AI-assisted technologies in the writing process

During the preparation of this work the authors used ChatGPT in order to assist with the translation of the manuscript from Spanish to English and with the grammatical adaptation of the text. After using this tool, the authors reviewed and edited the content as needed and take full responsibility for the content of the published article.

Funding sources

This research did not receive any specific grant from funding agencies in the public, commercial, or not-for-profit sectors.

Declaration of competing interest

The authors declare that they have no known competing financial interests or personal relationships that could have appeared to influence the work reported in this paper.

Appendix. Extended thermophysical data for representative hydrocarbon mixtures

This appendix provides a reduced set of supporting thermophysical data for the surrogate hydrocarbon mixtures used in the refinery integration analyses of Section 5. The purpose of the appendix is not to restate the mixture definitions already introduced in the main text, but to preserve traceability for the property calculations used in the energy, entropy, and exergy balances.

Thermodynamic properties – enthalpy (H), entropy (S), density (ρ), and specific heat (C_p) – were calculated using the `CoolProp` library (version 6.6.2) over a temperature range representative of refinery heating duties. In the present work, only property differences were used in the heat-balance and exergy calculations, so the absolute reference state of H and S does not affect the comparative results reported in Section 5 [22,23,47].

Table A.19 reports a compact set of temperature-dependent thermophysical properties for the representative heavy mixture used in the vacuum-heater analyses. These values are sufficient to document the property trends underlying the calculated cumulative heat–temperature curves and entropy-generation estimates.

Values are reported relative to the internal `CoolProp` reference state. Only differences in H and S were used for the energy and exergy balance calculations discussed in Section 5. The simplified mixture framework adopted in the main text should therefore be interpreted as a thermodynamic surrogate approach aimed at comparative integration analysis rather than detailed refinery assay reconstruction [25,48].

Data availability

No data was used for the research described in the article.

Table A.19
Temperature-dependent thermophysical properties of the representative heavy hydrocarbon mixture calculated with `CoolProp`, providing the basis for energy and exergy balance calculations in refinery integration analyses.

T (°C)	H (kJ/kg)	S (kJ/kg K)	ρ (kg/m^3)	C_p (kJ/kg K)	Note
30	−210.13	−0.463	702	2.17	Reference state
150	373.48	1.109	3.12	2.16	Atmospheric distillation range
300	738.37	1.843	2.25	2.69	Mid-temperature regime
420	1083.20	2.388	1.85	3.04	Vacuum distillation regime
480	1270.26	2.647	1.70	3.19	Upper bound of analysis

References

[1] International Energy Agency, Net zero by 2050: A roadmap for the global energy sector, 2021, URL https://www.iea.org/reports/net-zero-by-2050.

[2] United Nations, Net zero coalition, 2024, URL https://www.un.org/en/climatechange/net-zero-coalition.

[3] International Energy Agency (IEA), World Energy Outlook 2023, International Energy Agency, Paris, 2023, Licence: CC BY 4.0 (report); CC BY NC SA 4.0 (Annex A). URL https://www.iea.org/reports/world-energy-outlook-2023.

[4] Future Cleantech Architects, Decarbonizing High-Temperature Heat in Industry, Tech. Rep., Future Cleantech Architects, Remscheid, Germany, 2024, Technical report on pathways to decarbonize industrial high-temperature heat (500–2000°C). URL https://fcarchitects.org/wp-content/uploads/2024/10/FCA-Report-Decarbonizing-High-Temperature-Heat.pdf.

[5] L. Jing, H.M. El-Houjeiri, J.-C. Monfort, A.R. Brandt, M.S. Masnadi, D. Gordon, J.A. Bergerson, Carbon intensity of global crude oil refining and mitigation potential, Nat. Clim. Chang. 10 (2020) 526–532, http://dx.doi.org/10.1038/s41558-020-0775-3, Accedido el 2025-09-21. URL https://www.nature.com/articles/s41558-020-0775-3.

[6] É. Yáñez, H. Meerman, A. Ramírez, É. Castillo, A. Faaij, Fully integrated CO2 mitigation strategy for an existing refinery: A case study in Colombia, Appl. Energy 313 (2022) 118771, http://dx.doi.org/10.1016/j.apenergy.2022.118771, URL https://www.sciencedirect.com/science/article/pii/S0306261922002215.

[7] International Atomic Energy Agency, Nuclear Cogeneration for Climate Change Mitigation and Sustainable Development Goals, Tech. Rep., International Atomic Energy Agency (IAEA), Vienna, Austria, 2024, ISBN 978-92-0-119224-0 (Paperback); ISBN 978-92-0-119324-7 (PDF). URL https://www-pub.iaea.org/MTCD/Publications/PDF/TE-2056web.pdf.

[8] Nuclear Energy Agency, High-temperature Gas-cooled Reactors and Industrial Heat Applications, Tech. Rep., in: NEA No. 7629, Paris, 2022, http://dx.doi.org/10.1787/7406b814-en, URL https://www.oecd.org/en/publications/high-temperature-gas-cooled-reactors-and-industrial-heat-applications_7406b814-en.html.

[9] U.S. Department of Energy, High temperature reactors, in: Quadrennial Technology Review 2015: An Assessment of Energy Technologies and Research Opportunities, U.S. Department of Energy, Washington, DC, 2015, 4.J–1–4.J–24. Technology Assessment 4.J: High Temperature Reactors. URL https://www.energy.gov/sites/prod/files/2016/03/f30/QTR2015-4J-High-Temperature-Reactors.pdf.

[10] International Atomic Energy Agency, Small modular reactors: Advances in SMR developments 2024, in: Non-serial Publications, International Atomic Energy Agency, Vienna, 2024, http://dx.doi.org/10.61092/iaea.3o4h-svum, URL https://www-pub.iaea.org/MTCD/Publications/PDF/p15790-PUB9062_web.pdf.

[11] NuScale Power Corporation and Ebara Elliott Energy, Nuscale power and ebara elliott energy announce a strategic partnership to showcase use of advanced nuclear technology to power petrochemical plants, 2026, https://www.nuscalepower.com/press-releases/2026/nuscale-power-and-ebara-elliott-energy-announce-a-strategic-partnership-to-showcase-use-of-advanced-nuclear-technology-to-power-petrochemical-plants. Press release, 19 March 2026.

[12] Z. Zhang, Z. Wu, D. Wang, Y. Xu, Y. Sun, F. Li, Y. Dong, Current status and technical description of Chinese 2×250MWth HTR-PM demonstration plant, Nucl. Eng. Des. 239 (7) (2009) 1212–1219, http://dx.doi.org/10.1016/j.nucengdes.2009.02.023, URL https://www.sciencedirect.com/science/article/pii/S0029549309001332.

[13] Z. Zhang, Y. Dong, F. Li, Z. Zhang, H. Wang, X. Huang, H. Li, B. Liu, X. Wu, H. Wang, X. Diao, H. Zhang, J. Wang, The shandong shidao bay 200 MWe high-temperature gas-cooled reactor pebble-bed module (HTR-PM) demonstration power plant: An engineering and technological innovation, Engineering 2 (1) (2016) 112–118, http://dx.doi.org/10.1016/J.ENG.2016.01.020, URL https://www.sciencedirect.com/science/article/pii/S2095809916301552.

[14] A. Berens, F. Bostelmann, N.R. Brown, Equilibrium core modeling of a pebble bed reactor similar to the Xe-100 with SCALE, Prog. Nucl. Energy 171 (2024) 105187, http://dx.doi.org/10.1016/j.pnucene.2024.105187, URL https://www.sciencedirect.com/science/article/pii/S0149197024001379.

[15] U.S. Nuclear Regulatory Commission, Xe-100, pre-application activities for the x-energy xe-100 high-temperature gas-cooled reactor, 2025, URL https://www.nrc.gov/reactors/new-reactors/advanced/who-were-working-with/pre-application-activities/xe-100.

[16] R.S. El-Emam, R. Ajaj, K. Khlie, C. Zamfirescu, Decarbonizing petrochemical refineries using integration with small modular reactors – a thermodynamics and environmental analysis, Case Stud. Therm. Eng. 79 (2026) 107765, http://dx.doi.org/10.1016/j.csite.2026.107765.

[17] L.M. Larsen, I.G. Lantgios, R. Gonzales, F. Joseck, S. Lawrence, Technical and Economic Considerations for Uprate of Existing Nuclear Reactors with Cogeneration, Tech. Rep. INL/EXT-24-78810, Idaho National Laboratory, Idaho Falls, Idaho, 2024, URL https://lwrs.inl.gov/content/uploads/11/2024/07/UprateExistingNuclearReactors.pdf.

[18] V. Novotny, J. Kim, S.E. Creasman, L.D. Williams, D.M. Mikkelson, Preliminary process and instrumentation design of advanced reactor integration with refineries and hydrogen production facilities, Tech. Rep., Idaho National Laboratory (INL), Idaho Falls, ID (United States), 2024, http://dx.doi.org/10.2172/2305387, URL https://www.osti.gov/biblio/2305387.

[19] J.C. Vargas Terán, Estudio operacional de mezclas de gases que estabilice el suministro de energía al horno de la Topping U-150 de la refinería de Barrancabermeja, Universidad Industrial de Santander, Facultad de Ingenierías Fisicoquímicas, Escuela de Ingeniería Química, Bucaramanga, Colombia, 2016, URL https://noesis.uis.edu.co/server/api/core/bitstreams/4d5aa48f-d18e-48cf-a8e8-555c9f3d4db7/content.

[20] The Downstream Download, Barrancabermeja refinery, 2025, Consultado el 18 de diciembre de 2025. https://www.downstreamdownload.com/data/refineries/latin-america-refineries/barrancabermeja.

[21] N.E. Enciso Ramírez, Análisis tecnoeconómico de un sistema de generación de energía con reactores nucleares tipo SMR en Colombia, 2025, URL http://hdl.handle.net/11349/95961.

[22] A. Bejan, Advanced Engineering Thermodynamics, fourth ed., John Wiley & Sons, Hoboken, NJ, 2016.

[23] T.J. Kotas, The Exergy Method of Thermal Plant Analysis, Reprint ed., Krieger Publishing Company, Malabar, FL, 2013.

[24] F.P. Incropera, D.P. DeWitt, T.L. Bergman, A.S. Lavine, Fundamentals of Heat and Mass Transfer, Seventh ed., John Wiley & Sons, 2011, Standard reference for heat transfer principles including LMTD derivation.

[25] R. Smith, State of the art in process integration, Appl. Therm. Eng. 20 (15) (2000) 1337–1345, http://dx.doi.org/10.1016/S1359-4311(00)00010-7, URL https://www.sciencedirect.com/science/article/pii/S1359431100000107.

[26] Wood to design upgrades at Ecopetrol refinery for cleaner fuels production, Hydrocarb. Process. (2025) URL https://hydrocarbonprocessing.com/news/2025/06/wood-to-design-upgrades-at-ecopetrol-refinery-for-cleaner-fuels-production/. (Accessed 14 March 2026).

[27] U. Hamidu, S. Ahmed, U. Hamza, Energy integration of crude distillation unit of a refining and petrochemical company in northern Nigeria, J. Appl. Sci. Environ. Manag. 26 (11) (2022) 1803–1811, URL https://pdfs.semanticscholar.org/ee71/3785d1ff0cc8c1caa90b18c7d9cc8776da16.pdf.

[28] C. Cui, J. Sun, Coupling design of interunit heat integration in an industrial crude distillation plant using pinch analysis, Appl. Therm. Eng. 117 (2017) 145–154, http://dx.doi.org/10.1016/j.applthermaleng.2017.02.032, URL https://www.sciencedirect.com/science/article/pii/S1359431117308396.

[29] C. Fang, Q. Min, Y. Yang, Y. Sun, Process heat applications of HTR-PM600 in Chinese petrochemical industry: Preliminary study of adaptability and economy, Annals Nucl. Energy 110 (2017) 73–78, http://dx.doi.org/10.1016/j.anucene.2017.06.024.

[30] Y. Kansha, A. Kishimoto, A. Tsutsumi, Application of the self-heat recuperation technology to crude oil distillation, Appl. Therm. Eng. 43 (2012) 153–157, http://dx.doi.org/10.1016/j.applthermaleng.2011.10.022, Optimisation of Cogeneration and Energy Intensive Processes, Heat Transfer Enhancement, Industrial Applications – PRES 11. URL https://www.sciencedirect.com/science/article/pii/S1359431111005606.

[31] I.E.A. Greenhouse Gas R&D Programme, CO_2 Abatement in Oil Refineries: Fired Heaters, Tech. Rep. PH3/31, IEA Greenhouse Gas R&D Programme, Cheltenham, UK, 2000, URL https://publications.ieaghg.org/docs/General_Docs/Reports/Ph3_31%20Oil%20refinery%20fired%20heaters.PDF.

[32] U.S. Department of Energy, Energy Bandwidth for Petroleum Refining Processes, Tech. Rep., U.S. Department of Energy, Office of Energy Efficiency and Renewable Energy, Washington, DC, 2006, URL https://www.energy.gov/sites/default/files/2013/11/f4/bandwidth.pdf.

[33] J.H. Gary, G.E. Handwerk, M.J. Kaiser, Petroleum Refining: Technology and Economics, fifth ed., CRC Press, 2007.

[34] EPA, Chapter 5: Petroleum Refining — Vacuum Distillation, Tech. Rep., U.S. Environmental Protection Agency, 1995, URL https://gaftp.epa.gov/ap42/ch05/s01/final/c05s01_jan1995.pdf.
[35] A. Boretti, Hydrogen production by using high-temperature gas-cooled reactors, Int. J. Hydrog. Energy 48 (21) (2023) 7938–7943, http://dx.doi.org/10.1016/j.ijhydene.2022.11.269, URL https://www.sciencedirect.com/science/article/pii/S0360319922055872.
[36] T.R. Society, Nuclear cogeneration: Civil nuclear in a low-carbon future, 2020, Royal Society Report. URL https://www.royalsociety.org/-/media/policy/projects/nuclear-cogeneration/2020-10-7-nuclear-cogeneration-policy-briefing.pdf.
[37] Y. Brits, J. Crowell, X-Energy: XE-100 reactor – the key to an integrated energy system, 2020, https://www.nice-future.org/docs/nicefuturelibraries/default-document-library/x-energy.pdf?sfvrsn=e377b6fc_1. National Renewable Energy Laboratory, in: Flexible Nuclear Energy for Clean Energy Systems.
[38] S. Ecopetrol, Ecopetrol inauguró granja solar la iguana, un nuevo hito de autogeneración de energía renovable, 2025, URL https://www.ecopetrol.com.co/wps/portal/Home/es/noticias/detalle/ecopetrol-inauguro-granja-solar-la-iguana-un-nuevo-hito-de-autogeneracion-de-energia-renovable. (Accessed 14 March 2026).
[39] Ministerio de Minas y Energía de Colombia, Colombia's Hydrogen Roadmap, Tech. Rep., Ministerio de Minas y Energía, Bogotá, Colombia, 2021, URL https://www.minenergia.gov.co/documents/5862/Colombias_Hydrogen_Roadmap_2810.pdf.
[40] K. Kugeler, Z. Zhang, High-temperature gas–cooled reactor for process heat applications, first ed., in: Power Systems, Springer Singapore, 2025, p. XVI, 1492, http://dx.doi.org/10.1007/978-981-97-5540-0, 1196 b/w illustrations, 27 illustrations in colour. URL https://doi.org/10.1007/978-981-97-5540-0.
[41] F. Okamoto, K. Ohashi, Modular high-temperature gas-cooled reactor for expanding nuclear heat utilization, Fuji Electr. Rev. 56 (4) (2010) 134–139, URL https://americas.fujielectric.com/files/FER-56-4-134-2010.pdf.
[42] I.N. Laboratory, History and development of high temperature gas-cooled reactors, 2019, INL Training Material. URL https://art.inl.gov/NRC%20Training%202019/03_52882a_HTGR_History.pdf.
[43] U.S. Department of Energy, Office of Nuclear Energy, Benefits of small modular reactors (SMRs), 2023, URL https://www.energy.gov/ne/benefits-small-modular-reactors-smrs.
[44] C.L. Vinoya, A.T. Ubando, A.B. Culaba, W.H. Chen, State-of-the-art review of small modular reactors, Energies 16 (2023) http://dx.doi.org/10.3390/en16073224.
[45] B. Linnhoff, D.W. Townsend, D. Boland, G.F. Hewitt, B.E.A. Thomas, A.R. Guy, R.H. Marsland, A User Guide on Process Integration for the Efficient Use of Energy, Institution of Chemical Engineers, Rugby, UK, 1982.
[46] A.C. Dimian (Ed.), Chapter 10 pinch point analysis, in: Integrated Design and Simulation of Chemical Processes, in: Computer Aided Chemical Engineering, vol. 13, Elsevier, 2003, pp. 393–434, http://dx.doi.org/10.1016/S1570-7946(03)80034-2, URL https://www.sciencedirect.com/science/article/pii/S1570794603800342.
[47] I.H. Bell, J. Wronski, S. Quoilin, V. Lemort, CoolProp: Open-source thermophysical property database, 2014, https://coolprop.org/. Version 6.6.2, (Accessed 2025).
[48] G. Towler, R. Sinnott, Chemical Engineering Design: Principles, Practice and Economics of Plant and Process Design, third ed., Elsevier, Oxford, UK, 2022.
[49] J.H. Lienhard, J.H.V. Lienhard, A Heat Transfer Textbook, Dover Publications, 2019.
[50] R.K. Shah, D.P. Sekulic, Fundamentals of Heat Exchanger Design, John Wiley and Sons, 2003.
[51] Y.A. Cengel, M.A. Boles, Thermodynamics: An Engineering Approach, eighth ed., McGraw-Hill Education, New York, 2015.
[52] J. Hercog, J. Kupecki, B. Świątkowski, P. Kowalik, A. Boettcher, J. Malesa, E. Skrzypek, M. Skrzypek, D. Muszyński, G. Tchorek, Advancing production of hydrogen using nuclear cycles – integration of high temperature gas-cooled reactors with thermochemical water splitting cycles, Int. J. Hydrog. Energy 52 (2024) 1070–1081, http://dx.doi.org/10.1016/j.ijhydene.2023.06.333.
[53] T. Kim, D.-j. Kim, S.-D. Oh, H.-Y. Kwak, Energy, exergy and thermoeconomic analyses on hydrogen production systems using high-temperature gas-cooled and water-cooled nuclear reactors, Energies 16 (24) (2023) 8090, http://dx.doi.org/10.3390/en16248090.
[54] Y.T. Gómez Carvajal, D. Galeano, D. Morales, Techno-economic assessment of hydrogen production in Colombia using High-Temperature Gas-Cooled Reactors, Next Res. 8 (2026) 101516, http://dx.doi.org/10.1016/j.nexres.2026.101516.
[55] Colombia's Ecopetrol eyes 18 hydrogen projects, Arg. Media (2021) URL https://www.argusmedia.com/en/news-and-insights/latest-market-news/2259875-colombia-s-ecopetrol-eyes-18-hydrogen-projects. Accessed 14 march 2026.
[56] D.J. Kim, J.H. Kim, K.F. Barry, H.-Y. Kwak, Thermoeconomic analysis of high-temperature gas-cooled reactors with steam methane reforming for hydrogen production, Nucl. Technol. 176 (3) (2011) 337–351, http://dx.doi.org/10.13182/NT11-A13312.
[57] Y. Zhang, G. Hu, H. Zhang, Q. Liu, J. Zhou, Thermodynamic analysis and optimization for steam methane reforming hydrogen production system using high temperature gas-cooled reactor pebble-bed module, J. Nucl. Sci. Technol. 58 (12) (2021) 1359–1372, http://dx.doi.org/10.1080/00223131.2021.1951863.
[58] Y. Yoo, S.-Y. Lee, S.-H. Seo, S.-D. Oh, H.-Y. Kwak, Simultaneous production of pink and grey hydrogen using high-temperature (HT) gas-cooled nuclear reactors coupled with HT-electrolyzer and gas reforming unit, Int. J. Hydrog. Energy 102 (2025) 467–481, http://dx.doi.org/10.1016/j.ijhydene.2025.01.056, URL https://www.sciencedirect.com/science/article/pii/S0360319925000618.
[59] E.A.R. Molina, K.P. Sweeney, S.J. Root, N. Guaita, W.-C. Cheng, F.C. Joseck, L.T. Knighton, R.D. Boardman, Technical and Economic Assessment and Gap Analysis of Advanced Nuclear Reactor Integration with a Reference Oil Refinery: Technoeconomic Analysis for the Integration of Advanced Nuclear Power with a Reference Refinery, Tech. Rep., Idaho National Laboratory, Integrated Energy Systems, Idaho Falls, Idaho, USA, 2024, Prepared for the U.S. Department of Energy, Office of Nuclear Energy, under DOE Idaho Operations Office Contract DE-AC07-05ID14517. URL https://www.ies.inl.gov.
[60] J. Kupecki, J. Hercog, B. Świątkowski, E. Skrzypek, M. Skrzypek, A. Boettcher, G. Tchorek, Advancing production of hydrogen using nuclear cycles – integration of high temperature gas-cooled reactors (HTGR) with solid oxide electrolyzers (SOE), Int. J. Hydrog. Energy 53 (2024) 40–52, http://dx.doi.org/10.1016/j.ijhydene.2023.12.017.
[61] K. Hayashi, S. Kasahara, K. Kuribara, T. Nakagaki, X.L. Yan, Y. Inagaki, M. Ogawa, Process evaluation of use of high temperature gas-cooled reactors to an ironmaking system based on active carbon recycling energy system, ISIJ Int. 55 (2) (2015) 348–358, http://dx.doi.org/10.2355/isijinternational.55.348.
[62] Mitsubishi Heavy Industries, Development of high temperature gas-cooled reactor for hydrogen production system, Mitsubishi Heavy Ind. Tech. Rev. 61 (4) (2024) Available: https://www.mhi.com/technology/review/sites/g/files/jwhtju2326/files/tr/pdf/e614/e614090.pdf.